Microfluid Nanofluid (2007) 3:245–281
DOI 10.1007/s10404-007-0161-8

REVIEW

Digital microfluidics: is a true lab-on-a-chip possible?

R. B. Fair

Received: 10 February 2007 / Accepted: 14 February 2007 / Published online: 8 March 2007

Abstract The suitability of electrowetting-on-dielectric (EWD) microfluidics for true lab-on-a-chip applications is discussed. The wide diversity in biomedical applications can be parsed into manageable components and assembled into architecture that requires the advantages of being programmable, reconfigurable, and reusable. This capability opens the possibility of handling all of the protocols that a given laboratory application or a class of applications would require. And, it provides a path toward realizing the true lab-on-a-chip. However, this capability can only be realized with a complete set of elemental fluidic components that support all of the required fluidic operations. Architectural choices are described along with the realization of various biomedical fluidic functions implemented in on-chip electrowetting operations. The current status of this EWD toolkit is discussed. However, the question remains: which applications can be performed on a digital microfluidic platform? And, are there other advantages offered by electrowetting technology, such as the programming of different fluidic functions on a common platform (reconfigurability)? To understand the opportunities and limitations of EWD microfluidics, this paper looks at the development of lab-on-chip applications in a hierarchical approach. Diverse applications in biotechnology, for example, will serve as the basis for the requirements for electrowetting devices. These applications drive a set of biomedical fluidic functions required to perform an application, such as cell lysing, molecular separation, or analysis. In turn, each fluidic function encompasses a set of elemental operations, such as transport, mixing, or dispensing. These elemental operations are performed on an elemental set of components, such as electrode arrays, separation columns, or reservoirs. Examples of the incorporation of these principles in complex biomedical applications are described.

Keywords Lab-on-a-chip · Digital microfluidics · Biomedical applications · Detection · Analysis · Electrowetting

R. B. Fair (✉)
Department of Electrical and Computer Engineering,
Duke University, Durham, NC 27708, USA
e-mail: rfair@ee.duke.edu

1 Introduction

Historically, microfluidic devices have been designed from the bottom up, whereby various fluidic components are combined together to achieve a device that performs a particular application. Thus, just as component-level digital logic design has led to the development of processors and computers, microfluidic systems also have been motivated by component-level microfluidic devices. However, progress in microfluidic system development has been hampered by the absence of standard commercial components. Thus, many researchers have developed one-of-a-kind pumps, valves, detectors, flow sensors, etc. to pursue short-term research goals or to satisfy a specific application. But, these components are not widely available to designers like well-characterized, mass-produced, packaged logic gates. As a result, microfluidic systems built to date are highly specialized to a particular application, and are realized in custom technologies that may not be widely available. In addition, the general trend in commercial devices has been to fabricate simple, disposable devices that are designed to interface with an expensive box that houses the required control electronics, reagent supply, detectors, and pro-

gramming. Thus, the microfluidic device may perform only a limited set of operations, such as liquid transport, separation, or sensing. Then the device is used once and discarded.

To establish a development path (technology and commercialization) for microfluidics similar to the development of digital electronics requires the definition of architectural and execution concepts for assembling microfluidic devices into networks that perform fluidic operations in support of a diverse set of applications. Indeed, a hierarchical integrated microfluidic design approach has been described to facilitate scalable design for many biomedical applications (Zhang et al. 2002). The intent of this work was to raise the level of abstraction for performance modeling and simulation to the applications level, thus placing design concepts in the hands of the users rather than the technologists. The difficulty with this approach is the lack of standard fabrication technologies and microfluidic device simulation libraries, which make the hierarchical design approach difficult to implement, especially with continuous flow microfluidic systems. As a result, most of today's microfluidic devices are application specific, which requires that unique devices must be developed for each application with their own specific requirements. Also, since most of the work has been directed to microfluidic analysis systems, pre- and post-processing must be done off chip, requiring interfaces to external fluidic protocols.

Nevertheless, it is still a desirable goal to leverage microfluidic designs into multiple applications, which is the basis for the lab-on-a-chip concept. As it is with the equipment in a life sciences laboratory, each fluidic component performs a canonical operation. In this way, the complexity of the diverse set of biomedical applications can be reduced to a manageable set of fluidic operations. These operations can then be configured in various ways to realize a desired application (Jopling 2001). To accomplish such a lab-on-a-chip architecture it requires a hierarchical taxonomy. At the top level, applications are scaled to a microfluidic platform. The second level describes the microfluidic operations. And the third level describes the components to perform the operations. This manageable design approach is shown in Fig. 1. The modularity of the architecture allows flexibility of creating and choosing a collection of fundamental operations that meet the specific needs of a particular user (Jopling 2001).

The top level in Fig. 1 includes biomedical applications such as electrophoretic separations (Walker et al. 1998), DNA analysis (Schmalzing 1997; V-Dinh 1998), protein/enzyme analysis (Figeys et al. 1998), immuno- and bioassays (Abdel-Hamid et al. 1999; Delamarche 1997; Delamarche 1998; Ruzicka 1998), and pathogen detection (Ligler et al. 1998; Heim et al. 1999).

The second level of Fig. 1 decomposes the set of applications into common fluidic functions, such as liquid transport, mixing, filtering, and analysis. These operations serve as the canonical functions for creating various applications. These common operations determine the requirements for the set of microfluidic hardware components in the third level, such as buffers, channels, reservoirs, and mixers.

Of course, there are certain requirements for creating such a versatile architecture that is capable of accommodating multiple applications. First, the components must be integrated on a common substrate. That is, the components must be accessible by selective routing of reagents, depending on the need. There are various ways of doing routing, including programming before use (programmable hardware or modules) or reconfiguring devices on the fly (reconfigurable computing and electronic control). Second, the complexity of the microfluidic device will increase with the increase in versatility, making it less likely the user will want to pay to replace the device. This means that the device will need to be reusable with no cross-contamination among components or constituents. During operation, processing bottlenecks may occur at some heavily used

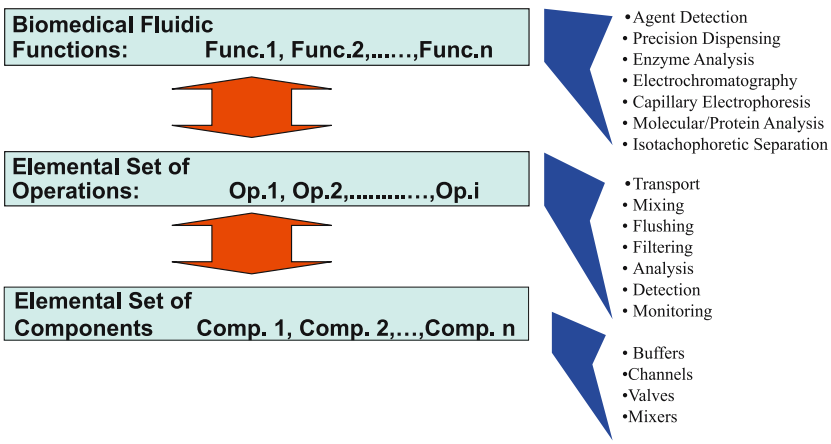

Fig. 1 Hierarchical design approach for implementing numerous applications on a common set of components

components, so resource allocation and redundancy will need to be determined.

In summary, the wide diversity in biomedical applications can be parsed into manageable components and assembled into an architecture proving the advantages of being programmable, reconfigurable, and reusable. This capability opens the possibility of handling all of the protocols that a given laboratory or a class of applications would require. And, it provides a path toward realizing the true lab-on-a-chip. However, this capability can only be realized with a complete set of elemental fluidic components that support all of the required fluidic operations. Architectural choices are described next.

1.1 Microfluidic architectural choices

The premise is that the extensive biomedical application base needs to be leveraged by expanding microfluidic operations into a complete system, or at least one that easily interfaces to off-chip protocols. To create such versatile microfluidic architecture it requires shared elemental fluidic operations on a common substrate (integration), reconfigurability, no cross-contamination, perhaps multitasking by components, and few bottlenecks. General classes of architecture include the chemical plant (reactants enter one end and products or waste exit the other end), the diagnostics architecture (bolus of liquid acted on to mimic human lab activity), or even computer architecture (transport buses, storage, processing units). Rather than review all of these architectures, this paper will address the diagnostic architecture as applied to discrete droplets of liquids, namely the digital microfluidic architecture.

Biochemical protocols for diagnostic procedures are typically based on fluid boluses. Petersen, however, pointed out that there are inefficiencies and complexities of implementing the bolus format on a microfluidic chip (Petersen et al. 1998). Rather, he proposed a continuous flow approach in which sample and reagent biochemical process are implemented in channels and synchronized. Small portions of the flowing sample are processed at a particular site as the sample stream passes. Nevertheless, building a reusable, synchronized microfluidic chip with the added requirements of reconfigurability and diagnostics capability would make a synchronized continuous flow device very complex.

1.2 Architecture for digital microfluidics

The concept of digital microfluidics arose in the late 1990s and involves the manipulation of discrete volumes of liquids on a surface. Manipulation of droplets can occur through various mechanisms, including electrowetting (Pollack et al. 2000; Lee et al. 2001; Cho et al. 2002), dielectrophoresis (Gascoyne and Vykoukal 2004), thermocapillary transport (Anton et al. 2003), and surface acoustic wave transport (Renaudin et al. 2004). In the digital microfluidic architecture the basic liquid unit volume is fixed by the geometry of the system (fluid quantization), whereas volumetric flow rate is determined by the droplet transport rate and the number of droplets transported. Thus, transport occurs in multiples of the minimum unit volume (fluid packetization). Unlike continuous flow systems, the minimum flow volume in a digital microfluidic system is not determined by the sensitivity of a flow sensor, since there is no flow sensor. Rather, minimum droplet volume is set by detector sensitivity (Manz et al. 1990).

The use of unit volume droplets allows a microfluidic function to be reduced to a set of basic operations. This ''digitization'' method facilitates the hierarchical taxonomy described above in Fig. 1 because numerous elemental fluidic operations can be accomplished with a common set of elemental components, i.e., combinations of electrodes on an array, as described below (Su et al. 2006). An example of digital microfluidic architecture is shown in Fig. 2. Depicted is a two-dimensional array of electrodes configured for an electrowetting-on-dielectric (EWD) system[1] (Ding et al. 2001).

Electrowetting-on-dielectric microfluidics is based on the actuation of droplet volumes up to several microliters using the principle of modulating the interfacial tension between a liquid and an electrode coated with a dielectric layer (Berge 1993). An electric field established in the dielectric layer creates an imbalance of interfacial tension if the electric field is applied to only one portion of the droplet on an array, which forces the droplet to move (Pollack et al. 2000). The architecture of Fig. 2 capitalizes on the flexibility of a unit flow grid array. At any given time, the array can be partitioned into ''cells'' that perform fluidic functions, such as storage, mixing, or transport. If the array is actuated by a clock that can change the voltage at each electrode on the array in one clock cycle, then the architecture has the potential for dynamically reconfiguring the functional cells at least once per clock cycle. Thus, once the fluidic function defined by a cell is completed, the cell is volatile and can be reconfigured.

Unlike continuous-flow microfluidic architecture, digital microfluidic architecture is under software-driven electronic control, eliminating the need for mechanical tubes, pumps, and valves. Protocols work similar to traditional bench-top

[1] Although electrowetting on dielectric has become known as EWOD (pronounced *e-wad*), perhaps a better designation would be EWD. A three letter designation with no vowels is less likely to be pronounced as an awkward word.

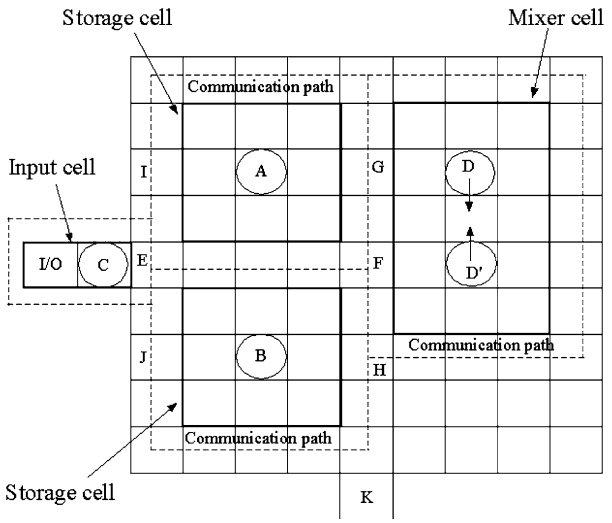

Fig. 2 Two-dimensional electrowetting electrode array used in digital microfluidic architecture (Ding et al. 2001)

methods, except with higher automation and significantly smaller sample sizes. Droplets can be merged, split, transported, mixed, and incubated by programming electrodes to carry out specific tasks. Thus, the advantages of the digital microfluidic architecture, when considered in light of real applications, are as follows (Fair et al. 2007):

- No moving parts: All operations are carried out between the two plates under direct electrical control without any use of pumps or valves.
- No channels are required: The gap is simply filled with liquid. Channels only exist in the virtual sense and can be instantly reconfigured through software.
- Many droplets can be independently controlled: Because the electrowetting force is localized at the surface.
- Evaporation is controlled/prevented: Depending on the medium surrounding the droplets.
- No ohmic current exists: Although capacitive currents exist, direct current is blocked, thus sample heating and electrochemical reactions are minimized.
- Works with a wide variety of liquids: Most electrolyte solutions will work.
- Near 100% utilization of sample or reagent is possible: No fluid is wasted for priming channels or filling reservoirs.
- Compatible with microscopy: The use of glass substrates and indium-tin-oxide (ITO) transparent electrodes makes the chip compatible with observation from a microscope.
- Extremely energy efficient: Nanowatts–microwatts of power per transfer.
- High speed: Droplet speeds of up to about 25 cm/s achieved.
- Droplet-based protocols are functionally equivalent to bench-scale wet chemistry: Thus established assays and protocols can simply be scaled down, automated, and integrated.
- Conditional execution steps can be implemented: Direct computer control of each step permits maximum operational flexibility.

It is the goal of this review to discuss electrowetting-based digital microfluidics in terms of its suitability for true lab-on-a-chip applications. In the sections below, the realization of various biomedical fluidic functions will be discussed in terms of implementation of elemental electrowetting operations on chip. The purpose here is to explore the types of applications that are possible using digital microfluidic architecture, and to describe these fluidic operations and their limitations. A detailed review of electrowetting basics can be found in the work of Mugele and Baret (2005Mugele and Baret 2005). In addition, work on simulation and modeling of droplet-based electrowetting has been reported by Zeng and Korsmeyer (2004), Zeng (2006), Lienemann et al. (2006), and; Walker and Shapiro (2006). Rather, here we describe operating characteristics of electrowetting devices and their usefulness or limitations. The discussion begins with a brief overview of the basics of actuating droplets by electrowetting on dielectric.

2 The digital microfluidic tool kit

Electrowetting on dielectric (EWD) is the phenomenon whereby an electric field can modify the wetting behavior of a polarizable and/or conductive liquid droplet in contact with a hydrophobic, insulated electrode. The application of an voltage between the liquid and the electrode results in an electric field across the insulator that lowers the interfacial tension between the liquid and the insulator surface according to the Lippman-Young equation (Mugele and Baret 2005). This effect is illustrated in Fig. 3. The application of a voltage to a series of adjacent electrodes that can be turned on or off creates an interfacial tension gradient that can be used to manipulate droplets (Pollack et al. 2000). Droplets are usually sandwiched between two parallel plates, the bottom being the chip surface, which houses the addressable electrode array, and the top surface being either a continuous ground plate or a passive top plate (the nature of the top plate is determined by chip's characteristics).

Figure 4 diagrams this setup. The chip surface is coated with an insulating layer of Paralyene C (~800 nm), and both the top and bottom surfaces are covered in a Teflon-AF thin film (~60 nm) to ensure a continuous hydrophobic platform necessary for smooth droplet actuation. A spacer

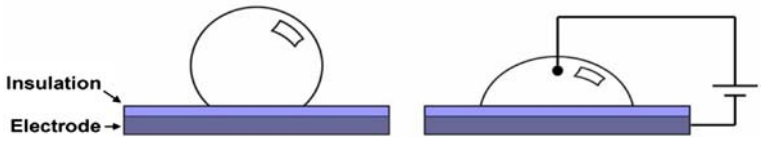

Fig. 3 The electrowetting-on-dielectric (EWD) effect. The droplet is initially at rest on a hydrophobic insulated electrode. Application of an voltage potential reduces the solid–liquid interfacial tension, resulting in improved wetting of the surface by the droplet. Typical voltages used are 20–80 V for the structure described below in Fig. 4

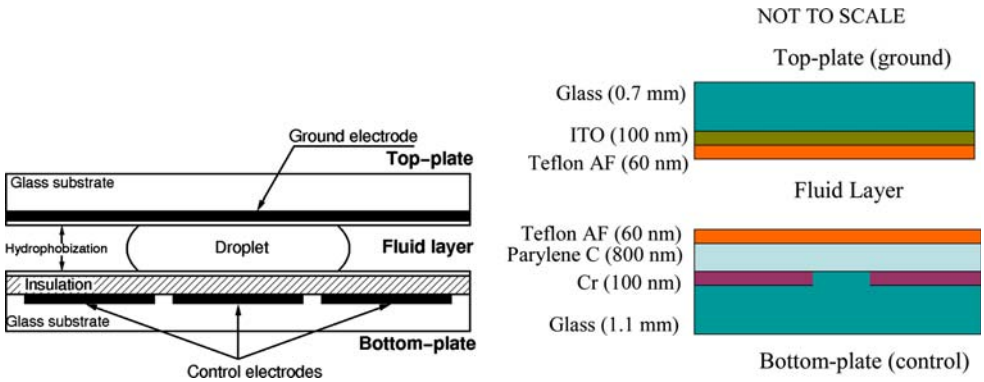

Fig. 4 Side-view of digital microfluidic platform with a conductive glass top plate (*left*). Materials and construction of the actuator (*right*). By adding a conductive top plate and adding individually addressed buried electrodes in the bottom plate, the droplet can be actuated from one electrode position to the next by the application of voltage

separates the top and bottom plates, resulting in a fixed gap height. The gap is usually flooded with silicon oil which acts as a filler fluid, preventing droplet evaporation and reducing surface contamination (Pollack et al. 2000). Other insulators have also been used in EWD devices, such as silicon dioxide with Teflon (Fowler et al. 2002; Moon et al. 2006) and Teflon alone (Seyrat and Hayes 2001).

Co-planar designs have also been developed where both the buried activation electrode and the exposed electrodes that ground the droplet are located on the bottom surface (Paik et al. 2004; Gong and Kim 2005; Pamula et al. 2005a, b; Cooney et al. 2006; Yi and Kim 2006). As shown in Fig. 5, the top plate is not required for coplanar devices, but its use is advised to contain the liquid medium and the droplets. Also, the passive top plate can be customized with specific chemistry or structures appropriate for each application. In this way, the top plate can be a disposable and processed independently of the microfluidic elements on the bottom surface. Realization of a co-planar design in printed circuit board (PCB) technology is illustrated in Fig. 5 with through-hole contacts that allow high density contacts to be made on the backside of the substrate. Typical threshold voltages for PCB EWD devices are in excess of 130 V due to the thick soldermask insulator (Paik 2006).

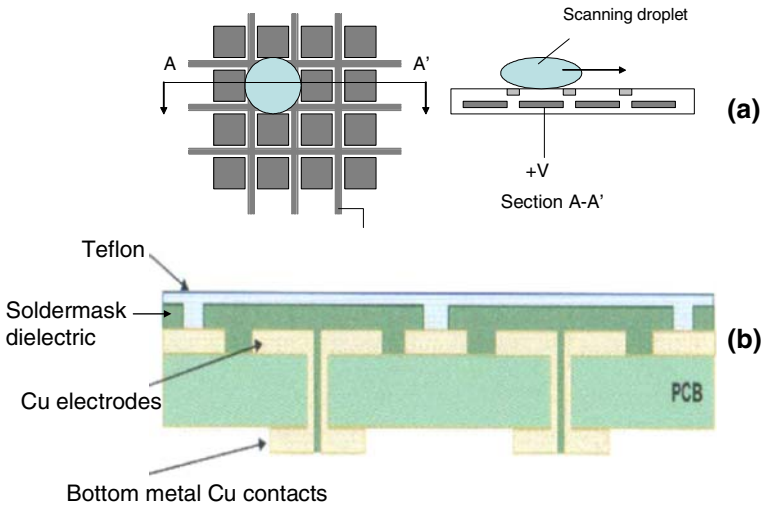

Fig. 5 **a** Coplanar actuation array for droplet scanning where electrical contact to the droplet is provided by surface electrodes, obviating the need for a top contact plate (Fair et al. 2004). **b** Co-planar construction in printed-circuit board technology (Paik 2006)

2.1 Realizable fluidic operations in EWD

2.1.1 Transport

Droplet transport is performed over contiguous electrodes, which connect different fluidic operations on chip. A detailed review of droplet transport mechanisms under EWD was recently published (Mugele and Baret 2005). And, classes of liquids that can be transported by EWD have been studied (Pollack 2001; Srinivasan 2005; Chatterjee et al. 2006). The basic EWD device is based on charge-control manipulation at the solution/insulator interface of discrete droplets by applying voltage to a control electrode. The device exhibits bilateral transport, is electrically isolated, uses a gate electrode for charge-controlled transport, has a threshold voltage, and is a square-law device in the relation between droplet velocity and gate actuation voltage. Thus, the EWD device is analogous to the metal-oxide-semiconductor (MOS) field-effect transistor (FET), not only as a charge-controlled device, but also as a universal switching element (Fair et al. 2001).

A comparison between a unit volume EWD device and a MOSFET is shown below in Fig. 6. Whereas the gate voltage of a MOSFET controls the drain current, the gate voltage of the EWD unit device applied to the electrode controls the mass transfer rate of a droplet, U. Liquid droplet motion can only be achieved above some threshold voltage, V_T. This observation is attributed to contact angle hysteresis: droplet motion can only be initiated when the contact angle on the leading (trailing) edge of the droplet exceeds (is smaller than) the local advancing (receding) contact angle (Mugele and Baret 2005). The threshold voltage for initiating droplet motion is found to decrease upon immersing the liquid droplet into an oil environment or by simply exposing a surface to oil and then drying the surface (Pollack 2001).

The transfer rates of droplets in an EWD device scale inversely with the electrode size (electrode pitch). Thus, a plot of average linear droplet velocity (pitch × rate) versus voltage gives a single curve (Fair et al. 2001). Droplet velocities have been achieved at approximately 100 mm/s at 60 V for droplets ranging in volume from approximately 1,000–1 nl. This corresponds to a rate of 666 Hz for a 3 nl droplet. When the larger droplets (>500 nl) were actuated at voltages higher than 60 V they would sometimes split apart. Fragmentation was not a problem for the smaller droplets, and velocities up to 250 mm/s were attained in some cases, although the high electric fields at these voltages (80–100 V) did tend to degrade the insulator over a short period of time.

Electrowetting-based droplet transport has been reported in a silicone oil medium (Pollack et al. 2000) and an air medium (Lee et al. 2001). Results are shown in Fig. 7 for the droplet transfer rate (Hz) in a EWD device, where transport was conducted in an air medium, in a silicone oil medium, and in air after the transport surface had been exposed to oil and then dried (Pollack 2001). It has been reported that impregnation of Teflon AF with silicone oil reduces the contact angle hysteresis of the surface (Verheijen and Prins 1999). It can be seen that droplet transport in silicone oil is improved (lower V_T) relative to transport in air. These results suggest that the differences are due largely to effects at the solid–liquid interface. In addition, it has been reported that threshold voltage increases with increasing silicone oil viscosity as well as increased viscosity of the droplet's liquid (Pollack 2001).

One reason for increased threshold voltage with increased silicone oil viscosity is entrainment of oil beneath the droplet. It was found theoretically by Quilliet and Berge (2002) that thin layers of the ambient oil 10–20 nm thick might form between a droplet and the substrate. This

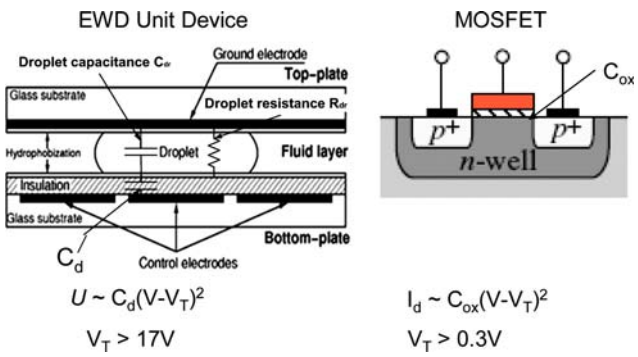

Fig. 6 Comparison between charge control devices: unit electrowetting device and a MOSFET

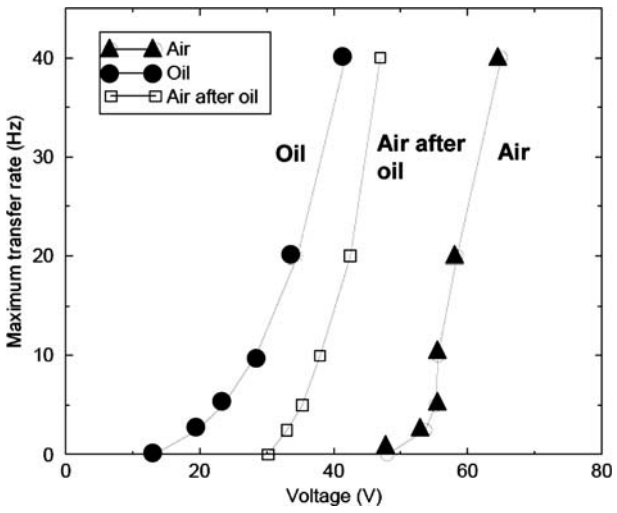

Fig. 7 Comparison of droplet transfer rates in a silicone oil medium, air medium, and air after oil exposure of the transport surface (Pollack 2001)

effect can be seen by comparing the measured capacitance of a droplet transported in an air medium with a droplet transported in a 1cSt silicon oil medium, as shown in Fig. 8. About 950 nl droplets of 100 mM KCl were transported across three electrodes, and the capacitance was dynamically measured on the center electrode (Fair et al. 2001). It can be seen in Fig. 8 that the capacitance of the droplet in oil exhibits a transient compared to the droplet in air. The slow rise in capacitance is believed to be due to entrained oil being squeezed out from beneath the droplet after the droplet has been transported. The time constant of the capacitance transient is about 2 s. When the oil viscosity was increased to 10cSt, the time constant was increased to about 6 s. The final thickness of oil beneath the droplet was sufficient to cause the capacitance to be about 25% lower in 1cSt oil than for the droplet in air.

The effect of entrained oil on the capacitance of a droplet in an EWD device is voltage dependent. Shown in Fig. 9 are the measured static capacitances of droplets in a EWD device where the areas of the droplets exceeded the area of the electrode. Whereas the capacitance of the large droplet in air is voltage independent and limited by the electrode area, the droplet in the oil medium has a strong voltage-dependent capacitance, which is limited by the variable oil thickness beneath the droplet. These results show a clear trend in oil that increasing the electric field increases droplet capacitance as the entrained oil thickness decreases with increase electrostatic pressure. It should be noted that at high electrode voltages, instabilities in the droplet capacitance in oil were observed, most likely due to the breakup of the oil into smaller oil droplets (Staicu and Mugeleet al. 2006).

Other variables that affect droplet transport through changing the threshold voltage are the thickness of the insulating layer over the electrode, the dielectric constant

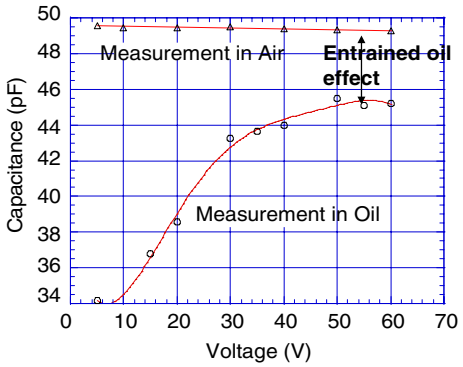

Fig. 9 Comparison of the static capacitances of droplets larger than the electrode area and either in air or immersed in a 1cSt oil medium (Fair et al. 2001)

and strength of the insulating layer, and the presence of a fluoropolymer layer, such as Teflon AF, over the insulator. Scaling the thickness of the insulator to increase the capacitance of the droplet/electrode system is limited by the dielectric strength of the insulator, whereby the increased electric field in the insulator may cause dielectric breakdown (Seyrat and Hayes 2001; Moon et al. 2002).

An insulator with a higher dielectric constant would lower the threshold voltage for electrowetting, but such materials may not be hydrophobic. Adding a top coat of fluoropolomer over the insulator makes the surface hydrophobic, but the voltage applied between the droplet and the electrode divides across the two insulators. For example, Teflon AF has a very low relative dielectric constant ($\varepsilon_{r2} = 1.9$). This means that the strength of the electric field in the Teflon AF overcoat would be ($\varepsilon_{r1}/\varepsilon_{r2}$) times larger than the electric field strength in the high dielectric constant insulator, where ε_{r1} is the dielectric constant of underlying insulator. Thus, breakdown of the

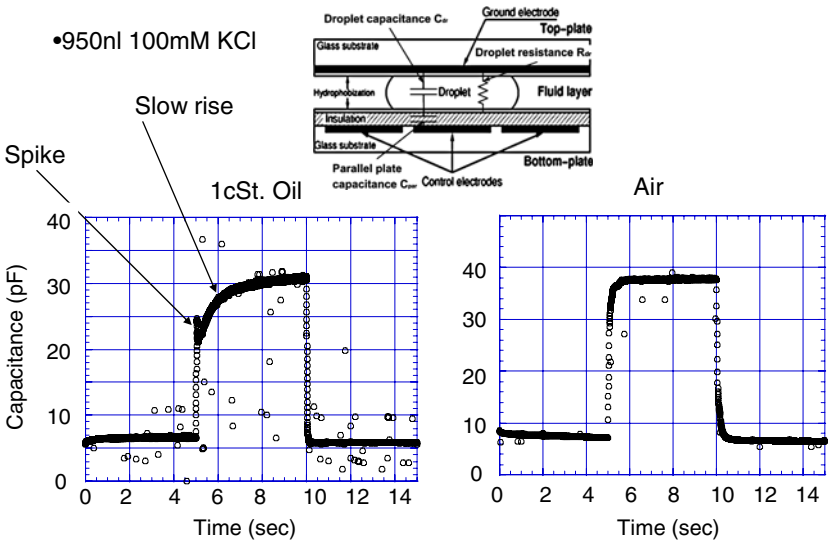

Fig. 8 Comparison of the dynamic capacitances of droplets transported in 1cSt silicone oil and in air (Fair et al. 2001)

fluoropolymer layer may occur first, which would cause the EWD device to fail by exposing the droplet to a non-hydrophobic surface.

In summary, little progress has been made in reducing the threshold voltage for EWD transport below the range of 15–20 V (Seyrat and Hayes 2001; Pollack 2001; Moon et al. 2002). It may be possible to find unique combinations of liquids, surfactants, and insulators that would allow lower voltage operation, but operation of lab-on-a-chip devices must occur with a variety of liquids. Thus, low voltage operation has not been a priority in current EWD device development for biomedical applications.

Another aspect of droplet transport is whether the applied actuation voltage is dc or ac (Jones et al. 2003). Pollack studied the transport of solvent droplets (acetone, chloroform, DMF, ethyl acetate, ethanol, ethyl ether, methanol, methynol, methylene C1, THF, toluene) in silicone oil (Pollack 2001). Whereas the solvents were miscible with silicone oil, he found that the solvent droplets could not be transported with dc electrode voltages applied. Nevertheless, the application of square-wave voltages (1–40 kHz) allowed for solvent transport. Subsequent studies have investigated ac-actuated transport of non-aqueous liquids in air (Chatterjee et al. 2006). Ac actuation has also been cited as being preferred over dc due to increased reliability in avoiding insulator charging with an alternating electric field. Today, most groups studying electrowetting transport use ac actuation.

If the ac frequency exceeds the hydrodynamic response time of the droplet, then the RMS value of the excitation voltage can be used in calculating contact angle and droplet velocity. Indeed measurements of the contact angle versus frequency of a demineralized water droplet showed a small variation at high frequency due to voltage drop due to impedance within the droplet (Mugele and Baret 2005).

Another advantage of ac actuation, that was recently found, is reduced dielectric hysteresis in the capacitance–voltage characteristic of a EWD device. A 5 µl, 100 mM KCl droplet in air was placed on an electrode larger than the droplet. A probe set at ground was inserted into the top of the droplet until it reached about one-fourth of the way down into the droplet. A voltage step sequence was then applied to this system to be able to see the effect of voltage on capacitance. This experiment allowed for variation in voltage step time, size of voltage step, and final voltage reached. Figure 10 shows the capacitance–voltage curve for a 50 V terminal voltage with a 250 ms interval and a 1 V dc step size. The increased voltage leads to a greater capacitance as the droplet wets the surface. This wetting leads to increased spreading of the droplet, which creates a greater surface area for the droplet at the interface with the insulator. Similar results were obtained in an oil medium (Nagiel 2006).

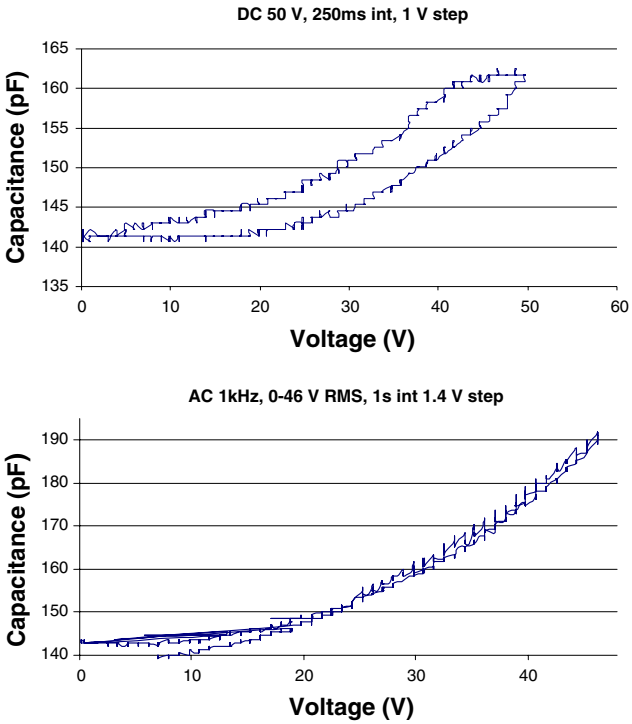

Fig. 10 C–V hysteresis of a droplet in air actuated with 1 V dc steps every 250 ms (*top*) compared with a droplet in air actuated with 1.4 V steps every 1 s up to 46 V RMS at 500 kHz (*bottom*)

The hysteresis shown under a dc bias in Fig. 10 is a real and reproducible effect. Its most likely cause is due to polarization within the insulator material covering the electrode, which does n'ot occur when an ac bias is applied. The insulator used in the experiments in Fig. 10 was Parylene-C coated with a thin layer of Teflon AF. Remnant polarization occurs as the dipoles in the insulator remained lined up causing negative charge to stay at the insulator interface with the liquid, thereby affecting wetting.

In biomedical applications it is required to transport biological liquids and beads. The transport of non-biological electrolytes using electrowetting has been demonstrated both in air (Cho et al. 2003) and in other immiscible media such as silicone oil (Pollack et al. 2002). And transport of polystyrene beads in solution (Srinivasan et al. 2003a, b) and magnetic beads (Fair et al. 2004) has been demonstrated. On the contrary, the transport of fluids containing proteins, such as enzyme-laden reagents and human physiological fluids, is not as straightforward. This is because most proteins tend to adsorb irreversibly to hydrophobic surfaces, and contaminate them. In the electrowetting system, the liquid droplet is sandwiched between two hydrophobic (Teflon AF-coated) plates. Any contact between the liquid droplet and the Teflon AF surface will therefore contaminate the surface. In addition to contamination, protein adsorption can also render the

surface permanently hydrophilic (Yoon and Garrell 2003). This is detrimental to transport, since electrowetting works on the principle of modifying the wettability of a hydrophobic surface, unless such contamination is intended for a particular application (Wheeler et al. 2005). Therefore any contact between a liquid droplet containing proteins and the Teflon surface should be avoided to prevent contamination and enable transport. As a consequence, air is not a suitable filler medium for assays involving proteins, since the droplet will always be in contact with the Teflon surface.

Silicone oil with its low surface tension and spreading property is an ideal alternative. The oil film beneath the droplet discussed above isolates the droplet from the Teflon surfaces, minimizing adsorption and facilitating transport. Srinivasan et al. (2003a, b, 2005) has studied the electrowetting transport in a silicon oil medium of droplets of whole blood, serum, plasma, urine, saliva, sweat, tears, and a buffer (0.1 M PBS, pH 7) for 25,000 continuous droplet transfers at 10 Hz to 40 min. The volumes of the droplets were between 1.3 and 1.5 µl, and transport measurements were made in a EWD device with 1.5 mm electrode pitch and 0.5 mm gap height with 1cSt silicone oil as the filler fluid. The droplet switching frequency of the various fluids is plotted versus dc switching voltage in Fig. 11. The general trend observed from Fig. 11 is that the liquids with less or no protein, such as buffer and saliva, transport more easily (lower voltage) than liquids such as blood or serum with high protein content. Indeed, the transport of protein solutions (BSA solution 10 mg/ml diluted to 1, 0.1, 0.01, and 0.001 mg/ml) confirmed this observation (Srinivasan 2005). Indeed, 10 mg/ml BSA could be transported under dc voltage actuation in 1cSt silicone oil, which is three orders of magnitude higher concentration than what was previously reported in air (Yoon and Garrell 2003).

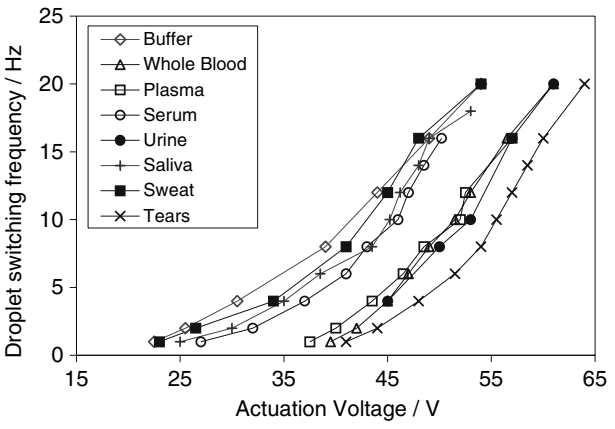

Fig. 11 Switching frequency of droplets of various physiological fluids as a function of applied dc voltage. (Srinivasan et al. 2003a, b)

Finally, to facilitate droplet transport on buses that connect various functional devices on chip, a multiphase bus design has been implemented to reduce the number of electrical contacts to the electrodes. In an *n*-phase bus every *n*th electrode is electrically connected, and droplets are always spaced apart by $k \times (n-1)$ electrodes, where k is any integer. This arrangement is illustrated in Fig. 12 for a four-phase bus. The use of a multiphase bus requires that droplet transport be synchronized, and this imposes constraints on parallel operations. Thus, optimized scheduling strategies are required to achieve the most efficient utilization of chip resources (Ding et al. 2001). Transport around corners must be carefully done to avoid droplet splitting, as shown in Fig. 12 (Srinivasan 2005).

2.1.2 *Fluidic I/O*

Loading samples and reagents on chip requires an interface between the microfluidic device and the outside world. Strategies for introducing samples and reagents onto a microfluidic chip are usually not discussed at length by workers in the field. Typically, droplets are pipetted onto EWD chips and then the top plate is applied to close the system (Pollack 2001; Wheeler et al. 2004). Fang discussed sample loading approaches for capillary electrophoresis (Fang 2004), and some of these concepts have been applied to an EWD device. The key is to provide a continuous-supply external source that keeps the on-chip reservoirs full.

The fluidic input port is challenging due to the large differences in the scales of real world samples (tens of microliters to milliliters) and the lab-on-a-chip (nanoliters to microliters). An additional problem for EWD devices that use an oil medium is the filler fluid, which creates the possibility of air bubbles being introduced during liquid introduction. Another requirement for fluidic ports is that liquid introduced into on-chip reservoirs should be contained for long-term storage and should not flow back out of the inlet. The two-plate EWD device depicted above in Fig. 3 is suitable for sample loading through a hole in the top plate. The loading hole is connected to the reservoir by a narrow channel of width, w, patterned in the spacer material that separates the top and bottom plates, as shown in Fig. 13 (Srinivasan 2005).

The principle of operation of the loading port in Fig. 13 is based on the pressure difference between the liquid in the reservoir and the narrow channel (Srinivasan 2005). From the LaPlace equation the liquid pressure in the reservoir is on the order of $\gamma\ (1/R + 1/h)$, where R is the radius of the reservoir, h is the height of the reservoir, and γ is the interfacial tension of the liquid with the surrounding media. Since $R >> h$, this reservoir pressure is approximately γ/h. The pressure in the narrow loading channel is

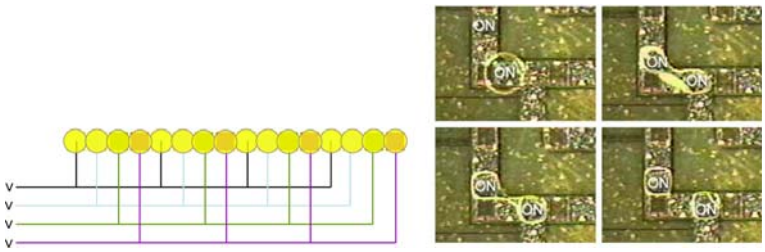

Fig. 12 Multiphase clocking for droplet transport on a bus (*left*). Splitting of a droplet in a three-phase clocking scheme as a result of the droplet ''seeing'' two electrodes turned on (*right*) (Srinivasan 2005)

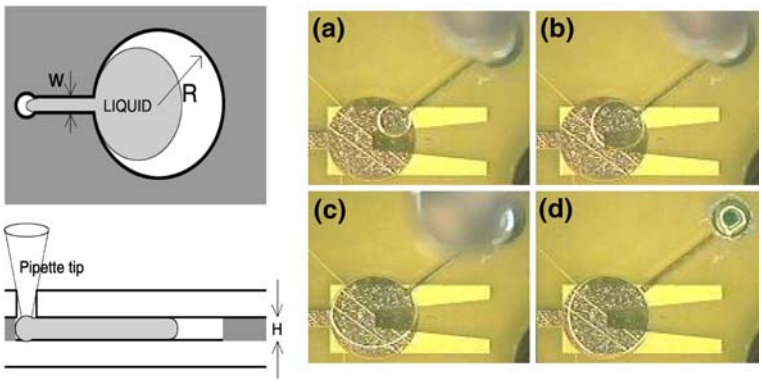

Fig. 13 Design of a manual loading port in a EWD device (*left*). Fabricated reservoir and loading port on an actual EWD device (*right*) showing the stages of pipetting liquid into an on-chip reservoir. (Srinivasan et al. 2004a, b)

γ $(1/w + 1/h)$. If w is kept small, then the pressure in the channel exceeds the reservoir pressure, and the liquid is forced to remain in the reservoir. The pipetting action initially overcomes this difference, allowing for the reservoir to be filled. The reservoir itself is an electrowetting device whose buried electrode is turned on during filling.

In the scheme described above, the microliter-sized reservoir serves as an interface to the nanoliter droplet-dispensing process that occurs on chip. As electrode dimensions on EWD devices are scaled down, direct dispensing of nanoliter and picoliter droplets from pipettes becomes impractical. Also, as the number of input ports increases, careful filling of reservoirs by hand also becomes impractical, particularly if the EWD device must interface with laboratory sample preparation procedures performed in 96 well plates. Thus, the well-plate format and the chip format are not compatible, and direct sample transfer from one format to the other requires serial liquid transfer, one well at a time. An alternative for parallel input-port sample loading is an electrowetting-based translator device. A microfluidic ''reformatter'' platform interfaces a well plate with the input ports of the EWD analysis chip (Fair et al. 2003; Srinivasan et al. 2004a, b). The droplet-based reformatter platform is an ideal microfluidic interface, since it is small, simple to control, and can be operated in a massively parallel fashion to increase throughput. There are also no moving parts and therefore no mechanical reliability problems.

Liquid is transferred from a well plate to the reservoirs on the electrowetting reformatter by applying pressure to the wells in a parallel fashion. Droplets are generated from the reservoirs using only electrowetting and/or external pressure and configured on the reformatter chip to match with the input port layout of the EWD chip. The droplets are then transferred on to the chip (Srinivasan et al. 2004a, b).

2.1.3 On-chip liquid storage and dispensing

Reservoirs can be created on EWD devices in the form of large electrode areas that allow liquid droplet access and egress (Fair et al. 2003; Wheeler et al. 2004; Srinivasan 2005; Moon et al. 2006). Liquids from the I/O ports are stored in reservoirs, such as those shown in Fig. 13. The basic lab-on-a-chip should have a minimum of three reservoirs—one for sample loading, one for the reagent, and one for collecting waste droplets, but this depends on the application. A fourth reservoir might be needed for a calibrating solution. Each reservoir should have independent control to allow either dispensing of droplets or their collection. Examples of on-chip reservoirs are shown in Fig. 14 (Srinivasan 2005; Moon et al. 2006).

Droplet dispensing refers to the process of aliquoting a larger volume of liquid into smaller unit droplets for manipulation on the electrowetting system. Droplet generation is the most critical component of an electrowetting-based lab-on-a-chip because it represents the world-to-chip interface. Controlled droplet dispensing on chip can occur by extruding a liquid finger from the reservoir through activation of adjacent serial electrodes (Ren et al. 2003a, b; Cho et al. 2003; Srinivasan 2005).

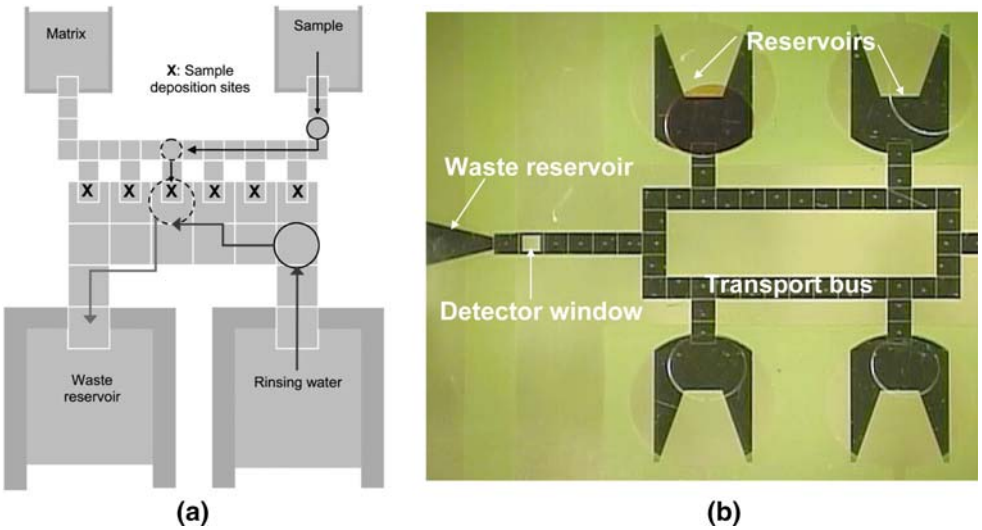

Fig. 14 **a** Drawing of an EWD device for MALDI-MS showing two 1 μl reservoirs and two 4 μl reservoirs (Moon et al. 2006). A die photo of a serial multiplexed assay EWD chip with one sample reservoir, one waste reservoir, and three reagent reservoirs (Srinivasan 2005)

A typical sequence of droplet dispensing is shown in Fig. 15 (Srinivasan et al. 2004a, b). Once the extruded liquid finger overlaps the electrode on which the droplet is to be formed, all the remaining electrodes are deactivated to form a neck in the column. The electrode in the reservoir is then activated to pull the liquid back, causing the neck in the finger to break and to form a droplet. The key to droplet dispensing is establishing the required internal pressure differences between the liquid in the reservoir and the front of the liquid finger.

According to the Laplace equation, the pressure in the liquid is subject to variations in the electrode geometry:

$$P - P_{\mathrm{a}} = \gamma_{\mathrm{LM}}(1/r - 1/R), \tag{1}$$

where γ_{LM} is the liquid–oil medium interfacial tension, r is the principal radius of curvature in the side view of Fig. 16, and R is the principal radius of curvature in the top view of Fig. 16.

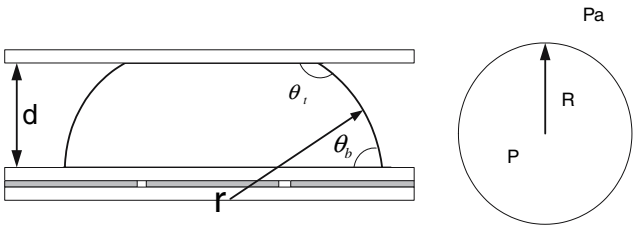

Fig. 16 Geometry of a droplet during electrowetting: side view (*left*) and top view (*right*)

Dispensing requires dynamic application of electrode voltages. To induce a protrusion of liquid from the reservoir requires that the electrowetting force must overcome the pressure gradient caused by curvature differences between the reservoir and the finger front. Referring to Fig. 17, this pressure difference can be expressed as (Ren et al. 2003a, b; Ren 2004):

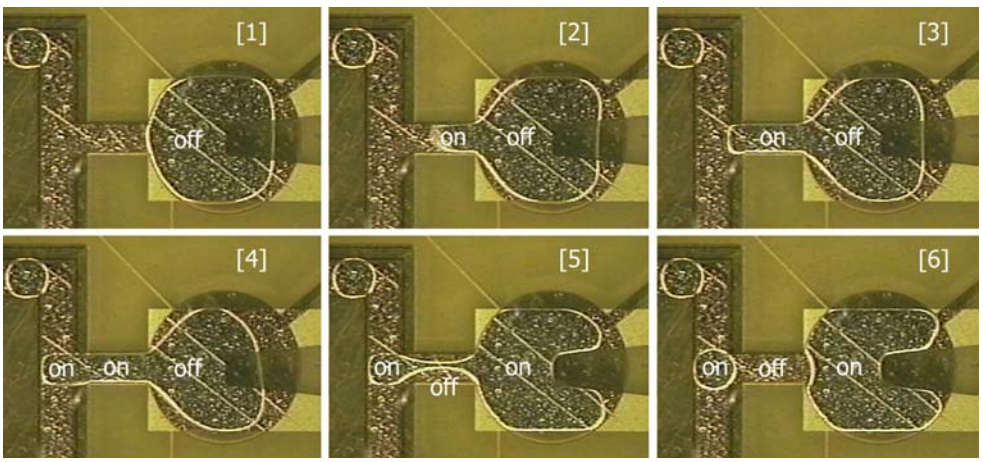

Fig. 15 Droplet formation from an on-chip reservoir (Srinivasan et al. 2004a, b)

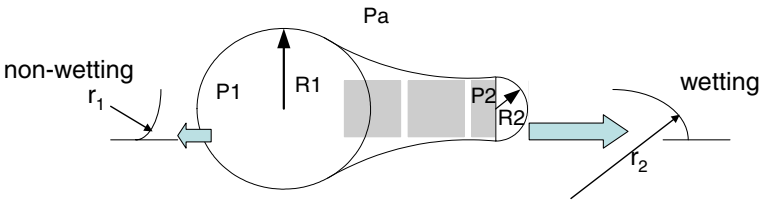

Fig. 17 Pressure in the reservoir when the reservoir electrode is off and the serial electrodes are turned on (Ren et al. 2003a, b)

$$P_2 - P_1 = \gamma_{LM}(\cos\theta_{b1} - \cos\theta_{b2})/d - \gamma_{LM}(1/R_1 - 1/R_2), \quad (2)$$

where θ_{b1}, θ_{b2} indicate the contact angle at the reservoir's bottom surface and finger front respectively, while R_1, R_2 indicate the principal radii of curvature, and d is the gap height in Fig. 16. Assuming a medium of silicone oil, then according to the equation of Lippmann and Young, the contact angle depends on the electrowetting actuation voltage V above the threshold voltage for actuation, V_T.

$$\cos\theta(V) - \cos\theta_0 = \varepsilon_0\varepsilon(V - V_T)^2/(2\gamma_{LM}t), \quad (3)$$

where $\theta(V)$, θ_0 indicate the contact angle with and without electrowetting, respectively, and t is the thickness of the insulator layer. By substituting Eq. 3 into 2, the static condition for liquid finger formation is described:

$$P_1 > P_2 \rightarrow 1/r_1 - 1/r_2 = \varepsilon_0\varepsilon(V - V_T)^2/(2\gamma_{LM}td) > 1/R_2 - 1R_1. \quad (4)$$

Thus, the pressure in the reservoir must be larger than the pressure in the protrusion, causing liquid flow into the protrusion. Equation 4 governs the liquid finger formation process and determines the required reservoir dimension, $2R_1$, and droplet size, $2R_2$ under a specified actuation voltage (Ren 2004).

At the initial application of voltage $V > V_T$ on the serial electrodes in frame four of Fig. 15 with the reservoir electrode off, the protrusion is formed due to electrowetting on the adjacent serial electrodes. The subsequent increase in the radius of curvature of the liquid at the front of the protrusion is due to a decrease in contact angle. If this pressure difference is large enough to overcome the contact angle hysteresis at the back end of the reservoir, the entire contents of the reservoir would be pulled out. Thus, to avoid actuation of the liquid out of the reservoir the following condition must be satisfied (Cho et al. 2003; Ren 2004):

$$0 < P_1 - P_2 < (\cos\theta_{b1} - \cos\theta_{b2})\gamma_{LM}/td. \quad (5)$$

Once the required pressure gradient has been formed for liquid protrusion, droplet pinch off must occur, which requires that the largest pressure occurs at the cutting point. This condition is illustrated in Fig. 18 and frame five of Fig. 15. It can be seen that the pressure gradient between the reservoir and the neck will depend on the number of electrodes over which the protrusion is drawn. Once the neck pinches off, liquid flows back to the reservoir and into the formed droplet (frame six of Fig. 15) (Ren et al. 2003a, b; Ren 2004).

For droplet formation in Fig. 18, the liquid in regions 1 and 3 can be sustained, whereas the liquid in region 2 is unstable. Thus, the liquid in region 2 has a tendency to flow back to region 1. Successful necking occurs when $P_2 > P_1$. Thus, referring to Fig. 18, the pinchoff condition requires that

$$P_2 > P_1 \rightarrow 1/r_2 - 1/r_1 = \varepsilon_0\varepsilon(V - V_T)^2/(2\gamma_{LM}td) > 1/R_1 - 1R_2. \quad (6)$$

These pressure relations can be modified by changing droplet size, changing the gap height, d, between the two plates of the actuator shown in Fig. 16, and changing the electrode voltages. Ren (2004) has shown that a large aspect ratio (droplet size/gap height = $2R_3/d$) and small droplet size are favorable for pinchoff of a droplet. Thus, the magnitude of the magnitude of the radius of curvature R_2 (negative) in Fig. 18 can be approximately expressed in terms of droplet radius R_3 and the number of electrodes in the pinchoff region:

$$|R_2| \approx (N^2 + 1)R_3/2. \quad (7)$$

Substituting Eq. 7 into 6 gives the condition

$$P_2 > P_1 \rightarrow 1/r_2 - 1/r_1 = \varepsilon_o\varepsilon(V - V_T)^2/(2\gamma_{LM}td) > 1/R_1 + 2/((N^2 + 1)R_3). \quad (8)$$

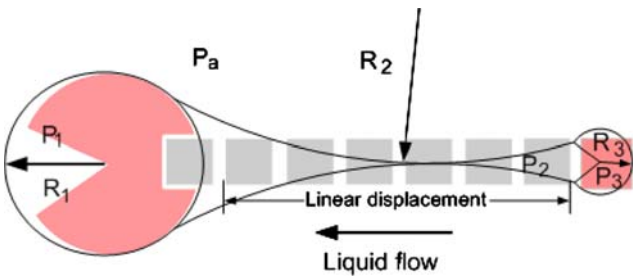

Fig. 18 Breaking of the liquid neck to form a droplet of radius R_3 (Ren et al. 2003a, b)

Equation 8 shows that for a fixed droplet size, a large aspect ratio EWD device requires fewer displacement electrodes, N. Using these concepts the conditions for successful droplet formation in a EWD device fabricated as described in Fig. 4 was analyzed (Ren 2004). For example, Fig. 19 shows the minimum actuation voltage versus the gap height to induce water-in-air protrusion from a 3 mm diameter reservoir on electrodes with a 500 μm pitch. Thus, dispensing is facilitated by a small gap height in the actuator. These results are insensitive to scaling as long as the aspect ratio (droplet size/gap height) is maintained. Thus, a 15 μm electrode pitch with a 5 μm gap height would have the same minimum actuation voltage for dispensing as a 500 μm pitch electrode with a 167 μm gap.

The minimum number of serial electrodes, N, for dispensing droplets from a reservoir has also been determined for 60 V dispensing of water in an oil medium, taking into account contact angle hysteresis. Again, the calculations were based on the structure described in Fig. 4 (Ren 2004). These results are exhibited in Fig. 20 which shows that as long as the aspect ratio of droplet size/gap height is greater than about six, that only one electrode is required for dispensing a droplet from a reservoir.

The reproducibility of on-chip dispensing has been studied as a function of the surface tension of the liquid in the reservoir (Ren et al. 2003a, b; Ren 2004). A total of 0.1 M KCl in water was dispensed with a nominal volume of 75 nl. As shown below in Fig. 21, the coefficient of variability was 3% over 16 droplets dispensed. The measured surface tension was 52 dynes/cm. In a second experiment, Triton X-100 was added with 0.01% concentration to reduce the interfacial tension to 10 dynes/cm. The coefficient of variation in dispensed droplet volume degraded to 12% over eight dispensed droplets. When a solution with concentration of 0.1% Triton X-100 was dispensed, the volume variation was 15% over six dispensed droplets. These results indicate that lowering the interfacial tension between the liquid and the silicone oil degrades dispensed droplet volume reproducibility. An explanation for this degradation is based on the observation that solutions with low interfacial tension quickly pinched off during dispensing. Therefore, the electrode shape and number have a reduced influence on defining the radius of curvature in the pinchoff region, R_2.

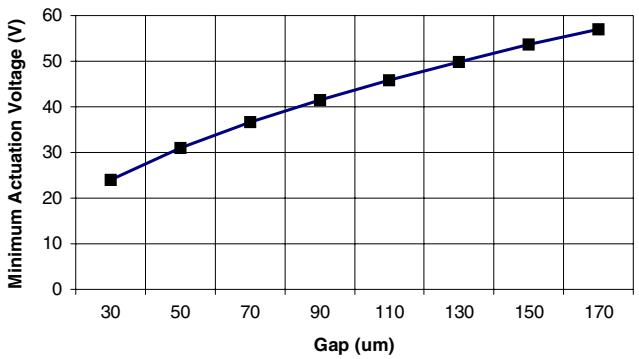

Fig. 19 Minimum actuation voltage versus gap height required to induce water-in-air protrusion from a 3 mm diameter reservoir onto 500 μm pitch size electrodes (Ren 2004)

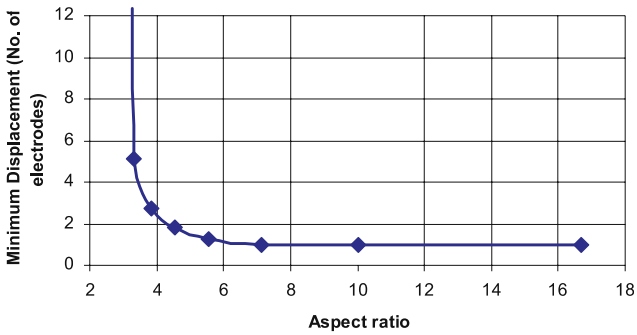

Fig. 20 Minimum number of electrodes for dispensing a droplet from a reservoir in a silicone oil medium versus aspect ratio, accounting for contact angle hysteresis (Ren 2004)

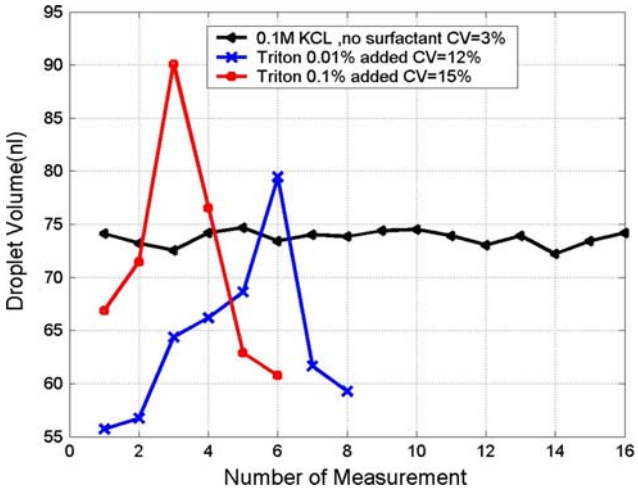

Fig. 21 Dispensed droplet variability as a function of surface tension (Ren et al. 2003a, b)

It was verified that the dispensed droplet volume and volume control depend on the number of serial electrodes attached to the reservoir, as shown in Fig. 22 (Ren 2004). The reproducibility of dispensing 0.1 M KCl solution with a three electrode dispenser was 1% compared to 3% for a two-electrode system. As noted above, the dynamics of forming a liquid protrusion and liquid flow during the necking of the protrusion depend on the number of electrodes.

Srinivasan (2005) has shown the repeatable and reproducible (CV < 2%) formation of droplets as small as 20 nL from an on-chip reservoir containing 0.5 μl of human

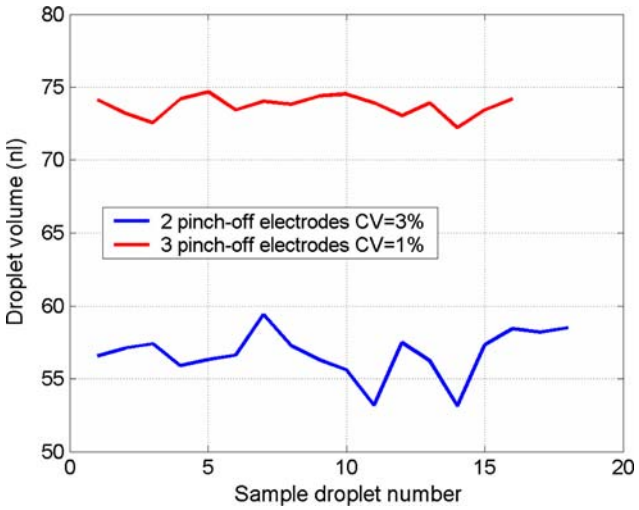

Fig. 22 Dispensed droplet volume control versus the number of serial electrodes interfaced to the reservoir (Ren 2004)

serum and plasma. The dispensing of protein solutions containing 10 mg/ml bovine serum albumin has also been demonstrated. (Srinivasan et al. 2004a, b).

Pressure-assisted droplet dispensing is a viable alternative to dispensing based solely on electrowetting. A capacitance feedback method has been demonstrated for controlled volume generation of droplets which is based on regulating the pressure of a dispensing nozzle in concert with electrowetting (Ren et al. 2003a, b). The reproducibility of 0.1 M KCl in water droplet volume was shown to be ±5% for dispensing rates that ranged from 8 to 45 droplets/min. And, by varying the droplet viscosity by a factor of 58, reproducibility was maintained at ±4%. In this scheme, no reservoirs are required on chip, but rather a pipette or small needle must be place over an electrode. As the liquid is dispensed onto the surface above the electrode, the capacitance between the liquid and the electrode is monitored. When the capacitance increases to a desired level, a feedback signal cuts off the liquid supply and the droplet moves off under electrowetting control. Figure 23 shows a pressure-assisted dispensing sequence (Ren et al. 2003a, b).

2.1.4 *Mixing*

Mixing of analytes and reagents in microfluidic devices is a critical step in realizing a lab-on-a-chip (Fowler et al. 2002; Hessel et al. 2004; Squires and Quakeet al. 2005). Mixing in these systems can either be used for pre-processing, sample dilution, or for reactions between samples and reagents in particular ratios. The ability to mix liquids rapidly while utilizing minimum area greatly improves the throughput of such systems. However, as microfluidic devices are approaching the sub nano-liter regime, reduced volume flow rates and very low Reynolds numbers make mixing such liquids difficult to achieve in reasonable time scales. In an electrowetting-based digital microfluidic device, for example, typical times to perform elemental fluidic operations can be compared with passive mixing solely by diffusion of the contents of two coalesced droplets. If the electrodes are clocked on or off in one cycle, then typical fluidic operations can be performed as follows:

- Droplet formation: three cycles
- Preprocess droplet splitting: one cycle
- Transport to a mixer: ten cycles
- Diffusional mixing in droplet: 1,000 cycles

As a result, active mixing is required in an EWD device to avoid bottlenecks in performing fluidic functions on chip.

Improved mixing relies on two principles: the ability to create turbulent flow at such small scales, or alternatively, the ability to create multilaminates to achieve fast mixing via diffusion (Fowler et al. 2002; Paik et al. 2003a, b). Most of the research has been focused on the second

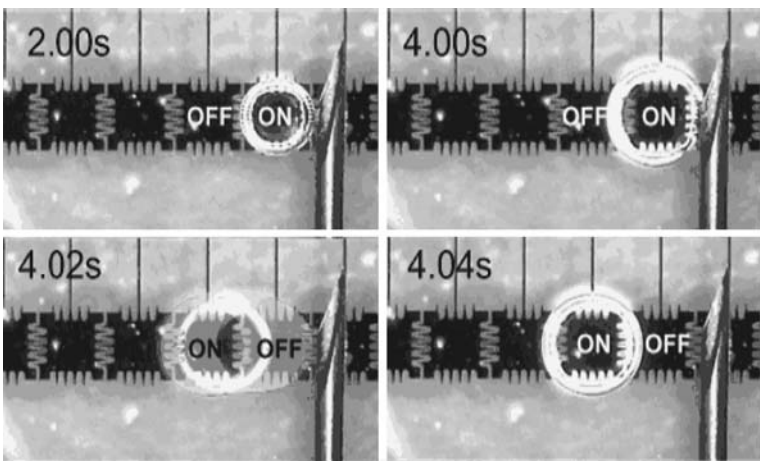

Fig. 23 Time lapse pictures of one droplet of 0.1 M KCl formed in 1cSt. silicone oil from a 300 μm diameter needle on a chip with 1 mm electrode pitch and 400 μm gap height. The electrical activation sequence of the electrodes is indicated. Generation rates up to 120 droplets/min were observed (Ren et al. 2003a, b)

principle, since turbulent flow would require the liquids to travel at high velocities or to introduce energy into the flow from an external source.

Hosokawa et al. (1999a, b) have demonstrated mixing of droplets in a hydrophobic microcapillary valve device where the droplets were formed, actuated, and mixed with the help of air pressure. Pamula et al. (2001) reported a passive droplet mixer where the droplets were actuated to coalesce only, but no external energy was introduced into the system after droplet coalescence. However, the layered, segregated structure within the merged droplet does not produce fast mixing. Fowler et al. (2002) have claimed fast droplet mixing using electrowetting-on-dielectric actuation to roll coalesced droplets to double the number of interfacial layers.

Active mixing of a coalesced droplet by transport across a programmed electrode path has been proposed (Paik et al. 2003a, b; Fan et al. 2003). Mixing times decrease as the number of electrodes on which a droplet moves increases (Paik et al. 2003a, b). Further improvement is obtained by increased droplet transport speed. Such improvements overcome flow reversibility associated with laminar flow. For example, shuttling a coalesced droplet over a two electrode linear array exhibits reversible flow. In Fig. 24, a fluorescein droplet was coalesced with a water droplet and then shuttled back and forth over adjacent electrodes. The flow patterns after each pass are shown (Paik et al. 2003a, b).

Mixing results on 2two, 3three, and 4 four electrode linear arrays are shown in Fig. 25 as a function of electrode switching frequency (Paik et al. 2003a, b). The fluorescent droplet contained 1 mM fluorescein (JT Baker), 0.125 M KCl to make the droplet conductive, and 0.125 M NaOH to maintain the proper pH for fluorescence. The non-fluorescent droplets contain 0.125 M KCl and 0.125 M NaOH only. For all active mixing experiments, a 600 μm gap was used, with 1.32 μl droplets and an actuation voltage of 50 V. All experiments were performed with 1cSt silicone oil as the filler liquid. Two CCD cameras were used in all the experiments to view the top and side views of the droplet simultaneously. The fluorescent droplets were excited with a tungsten lamp with a blue filter (490 nm). Both cameras were mounted with long pass filters (>510 nm) to collect fluorescence. The video was recorded onto SVHS tape and later digitized at 30 frames/s, such that the top and side views were perfectly synchronized. All experiments were recorded well past a subjective assessment of mixing for later analysis.

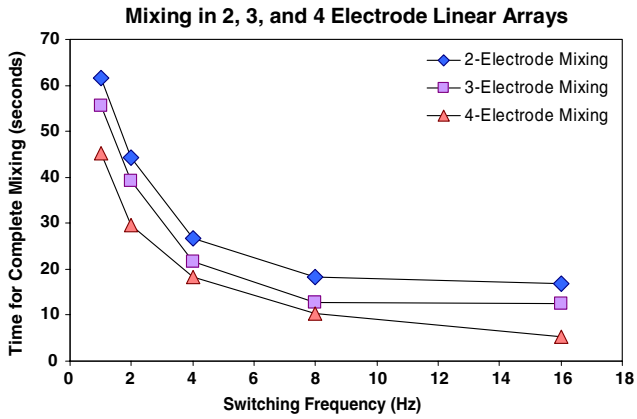

Fig. 25 Two, three, and four electrode linear array droplet mixing as a function of electrode voltage switching frequency (Paik et al. 2003a, b)

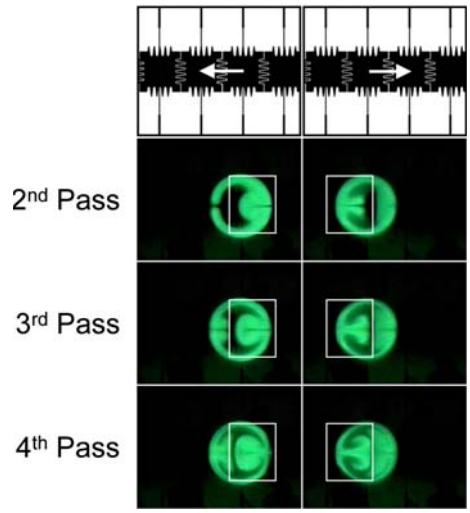

Fig. 24 Reversible flow in a coalesced droplet mixed in a two electrode linear array (Paik et al. 2003a, b)

Improved mixing results were obtained by using a $2 \times n$ array of electrodes. For example, droplet mixing on a 2×4 electrode array follows a pattern indicated in Fig. 26 and

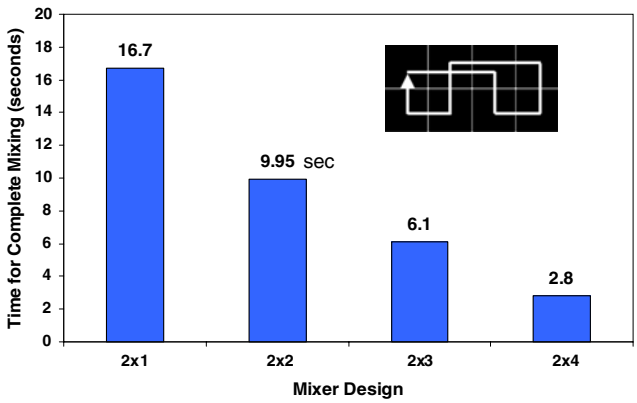

Fig. 26 Two dimensional array mixing results showing times for complete mixing according to the size of the array. The 2×4 transport pattern is shown as an *insert* in the figure (Paik et al. 2003a, b)

results in a mixing time of 2.8 s. Results on other $2 \times n$ arrays are also shown in Fig. 26 (Paik et al. 2003a, b). The mixing times are also affected by the aspect ratio of the EWD device, defined inversely here from the discussion above on dispensing as (gap height/electrode pitch). Aspect ratio dictates the shape of the droplet, which in turn affects mixing times. Thus, higher aspect ratios result in more spherical droplets, whereas low aspect ratios result in cylindrical droplets.

Mixing times in droplets are shown in Fig. 27 with increasing aspect ratio for a fixed electrode pitch of 1.5 mm at a switching frequency of 16 Hz (Paik et al. 2003a, b) The volume of the droplets for each experiment was adjusted to maintain the 1.5 mm electrode pitch. Mixing was performed on a four electrode linear array. Mixing times initially decrease with increasing gap height, most likely due to a lessening of the restriction on flow within the droplet. The minimum mixing time was achieved with an aspect ratio of about 0.4, after which mixing times increases slightly. This increase is due to the larger droplet volume required with the larger gap height.

When mixing data from different investigations are compared on a semi-logarithmic plot of the ratio of mixing volume to mixing time versus mixing area, the results obtained for linear array mixing and 2×2 array mixing fall on the trend line shown below in Fig. 28 (Harrison et al. 1996; Koch and Chatelain 1998; Hosokawa et al. 1999a, b; Liu et al. 2000; Hinsmann and Haberkorn 2001; He et al. 2001; Chou et al. 2001; Rohr et al. 2001). But, a significant deviation from this trend line is seen for the irreversible flow results obtained in Fig. 26 for the 2×4 array. The ratio of volume/(mixing time) is 100-fold higher for a 1 mm^2 mixing area than is indicated by the trend line and the results of Rohr et al. (2001) who modified a continuous-flow channel surface to render it porous through photo polymerization to facilitate mixing.

Recently, two groups have proposed the use of electrowetting to trigger self-excited oscillations of sessile droplets which cause the contact angles of the droplets to vary periodically between ~130° and 80° with a frequency between 10 and 125 Hz (Aizenberg et al. 2006; Mugele et al. 2006). The mixing process is based on the droplet having a free surface in a single plate EWD device which is contacted by a ground wire immersed into the droplet. The application of an electrode voltage causes the droplet to flatten until a capillary neck is formed between the wire and the droplet, which breaks above a certain voltage. The discharged droplet then returns to its initial shape.

Experiments with self-excited oscillation mixing show improved mixing times relative to passive diffusional mixing of up to a factor of 100 over a wide range in viscosity for 1–2 μl droplets, which translates to mixing times of about 3–50 s. An estimate of where these results fall on the chart in Fig. 28 is shown (Mugele et al. 2006), and it can be seen that mixing is very competitive. The advantage of mixing by self-excited oscillations is that mixing occurs

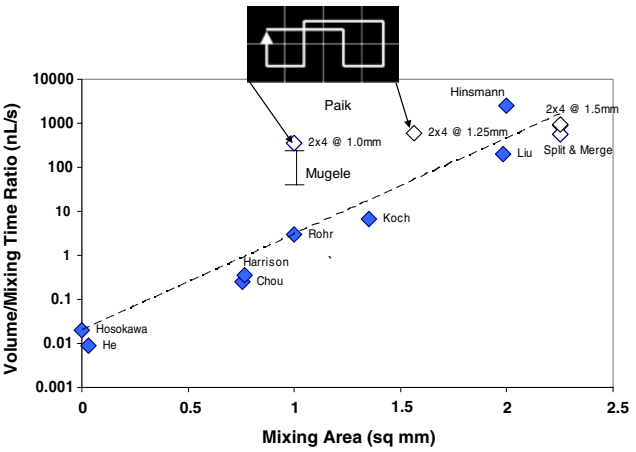

Fig. 28 Data from numerous liquid mixing studies showing the ratio of volume mixed (nl) to time (s) ratio plotted versus the mixing area (mm^2). Most of these data fall on a common trend line. However, the mixing protocol involving 2×4 array mixing produced unexpected improvements and a break from the trend

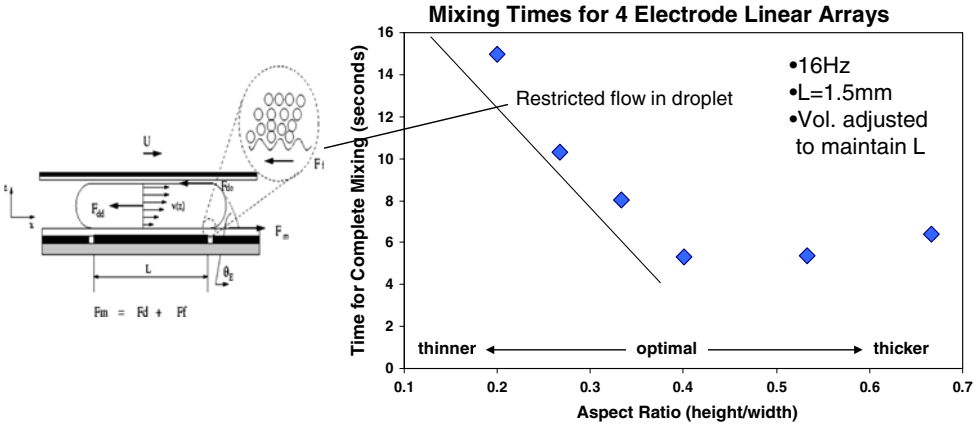

Fig. 27 Droplet mixing time for fixed electrode pitch and switching frequency as a function of aspect ratio, with gap height increasing from left to right (Paik et al. 2003a, b)

on a single electrode site. However, the method cannot be used if an EWD device has a top plate that constrains the vertical movement of the droplet, as shown above in Fig. 4. However, single plate EWD devices have disadvantages, including droplet evaporation and the inability to split droplets (Cooney et al. 2006).

In summary, active droplet-based mixing at high switching rates on a liner array of electrodes is at least an order of magnitude faster than passive diffusional mixing. Improved results can be obtained by mixing on two-dimensional arrays, which reduce reversible flow within the droplet. And an optimal aspect ratio has been observed that produces the fastest mixing results in two-plate EWD devices. Nevertheless, in many applications, such as the serial multiplexed assay device shown above in Fig. 14, the long transport bus will serve as an effective mixer as the coalesced droplet is transferred from any of the reagent reservoirs to the detector as it traverses over numerous electrodes in one direction.

2.1.5 *Droplet splitting and merging*

Perhaps, the simplest fluidic operations in an EWD device are the splitting of a droplet and the merging of two droplets into one. For splitting a droplet three electrodes are used as described by Cho et al. (2002) and described in Fig. 29. During splitting the outer two electrodes are turned on (Fig. 29c) and the contact angle θ_{b2} is reduced, resulting in an increase in the radii of curvature r_2. With the inner electrode off, the droplet expands to wet the outer two electrodes. As a result the meniscus over the inner electrode contracts to maintain a constant volume (Fig. 29a). Thus, the splitting process is underway as the liquid forms a neck with radius R_1. In general, the hydrophilic forces induced by the two outer electrodes stretch the droplet while the hydrophobic forces in the center pinch off the liquid into two daughter droplets (Berthier et al. 2006).

The criteria for breaking the neck in Fig. 29a is (Cho et al. 2001)

$$1/R_1 = 1/R_2 - (\cos\theta_{b2} - \cos\theta_{b1})/d, \quad (9)$$

where the symbols are indicated in Fig. 28. According to Eq. 9, necking and splitting are facilitated when the gap height, d, is made smaller or the volume of the droplet is increased.

However, it is often the case that even though the criterion in Eq. 9 is established, non-uniform splitting occurs. That is, the two droplets that result have different volumes. Generating droplets of uniform volume is critical in controlling the accuracy of fluidic processes such as dilution. Ren tested the reproducibility of the volume in droplet splitting over a range of 1.2–3.2 μl using a EWD device with 1.5 mm electrode pitch and gap height of 140 μm. The volume variation (volume after splitting divided by total volume) was about 7% (Ren 2004). Variables in the splitting process that affect uniformity include aspect ratio (electrode pitch/gap height), droplet/oil interfacial tension, electrode shape, time sequencing of electrode voltages, droplet alignment at the initiation of necking, and contact angle saturation. An example of non-uniform droplet splitting is shown in Fig. 30 (Ren 2004).

2.2 Fluidic functions based on EWD digital microfluidic operations

Referring back to Fig. 1, the basic EWD fluidic operations have been discussed, including transport, fluidic I/O, on-chip storage and dispensing, mixing, and droplet splitting.

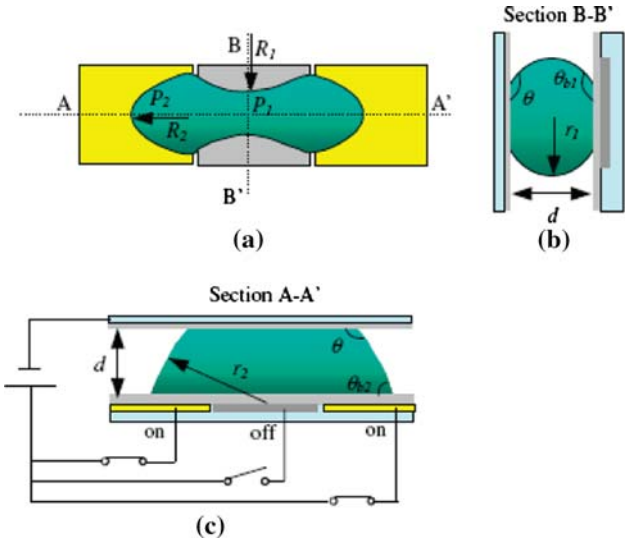

Fig. 29 Droplet configuration for splitting (Cho et al. 2002)

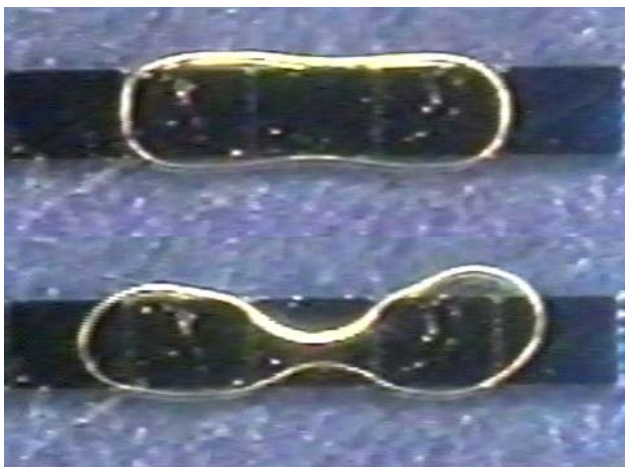

Fig. 30 Time-elapse photo of a droplet splitting process (Ren 2004)

These operations are performed on elemental fluidic components that are based on individual electrodes or combinations of electrodes. In this section, combinations of EWD components and functions are applied to microfluidic operations, including the following: sample dilution and purification, molecular separation, assays, PCR, and DNA sequencing. For each fluidic function, examples are given of experimental architecture and implementations, results, and issues.

2.2.1 *Sample dilution and purification*

Dilution of samples is an important step in almost all bioanalytical systems. The dilution step is done as part of the sample preparation process (pre-reaction) and/or during the reaction by controlling sample and reagent volumes. Sample dilution is done primarily for two reasons: to reduce the effect of interfering substances and to increase the linear range of operation of devices. A typical example is the enzymatic glucose assay (Trinder's reaction) where a dilution factor of 200 or more is used for the reaction to be linear up to glucose concentrations of 40 mM. In the case of the glucose assay the dilution is typically done by mixing a small volume (50 µl) of the sample with a large volume of reagent (1 ml). Sample glucose concentrations greater than 40 mM are typically pre-diluted with buffer.

In continuous flow microfluidic systems, on-chip chemical mixing ratios are typically determined by varying the sample flow rates of pre-concentrated reactants that enter a T-junction (Jacobson et al. 1999). However, accurately performing large dilutions are difficult, partly due to the fact that the relative pressure/voltage required is dependant on the properties of the fluid and geometry of mixing chambers/channels.

In EWD devices droplet-based dilution has been investigated using a binary interpolating mixing algorithm and architecture (Ren et al. 2003a, b; Fair et al. 2003; Griffith et al. 2006). The mixing of a unit sample droplet of concentration C and a unit buffer droplet results in a droplet with twice the unit volume, and a concentration of $C/2$. Splitting this larger drop results into two unit droplets of concentration $C/2$. Continuing this step in a recursive manner using the diluted droplet as the sample, an exponential dilution of 2^N can be obtained in N steps. This twofold dilution step can be extended to two droplets of different concentrations $C1$ and $C2$. This would result in two unit droplets with an interpolated concentration of $(C1 + C2)/2$ each. By cascading the exponential and interpolating dilution steps in a serial fashion, arbitrary dilution factors can be obtained. Using the interpolating serial dilution method, a large number of dilution factors can be obtained with a relatively small number of dilution (mixing/splitting) cycles. Using less than 10 such cycles one can obtain 38 different dilution factors in the range of 2–64.

Dilution is challenging in any microfluidic technology, and EWD is no exception. Ren et al. conducted dilution experiments in a silicone oil medium which included dispensing a sample droplet containing a 0.1 M KCl solution with 0.01% Triton X-100 surfactant colored with a red food dye. A buffer droplet was also dispensed and contained 0.1 M KCl and 0.01% Triton X. Mixing and splitting steps were done on a linear electrode array. The concentration of the mixed droplet was measured using optical absorbance. Images of the droplets were captured using a CCD video camera to obtain information about the volume variation. Due to the absence of a storage units on the chip, only exponential 2^N dilution factors were tested for $N = 1$, 2, and 3 (Ren et al. 2003a, b).

The interpolating serial dilution architecture was tested for dilution factors of 2, 4, and 8. In Fig. 31 is shown the inverse of the absorbance (1/concentration) as a function of the dilution factor. The straight lines in the plots correspond to the absorbance expected in the case of ideal dilution without any errors. The 'Δ' (delta) data represent the measured absorbance data, and '×' (cross) data corresponds to the expected absorbance, with a correction factor applied to account for volume variations. The deviation of the dilution factor from the ideal is ~15% for a dilution factor of 4 and 29% for a dilution factor of 8 (Ren et al. 2003a, b). This result represents a ~8% error in each dilution step. About 80% of this error was attributed to droplet volume variation in droplet splitting.

The experiments of Ren et al. were likely affected by the addition of 0.01% Triton X-100, which lowered the interfacial tension between the droplet and the silicone oil. As shown above in Fig. 21, droplet volume reproducibility of dispensed droplets with 0.01% Triton X-100 degraded to

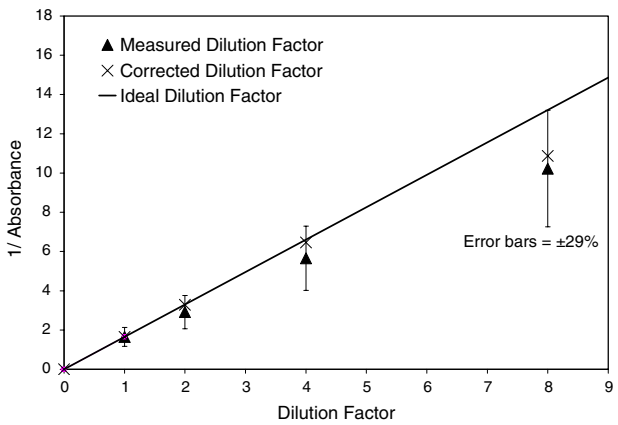

Fig. 31 Plot of expected versus measured dilution for dilution factors of 2, 4, and 8. (Ren et al. 2003a, b)

~12%. Schwartz et al. have shown that non-uniform surfactant distributions on small sessile droplets on a surface can cause deformation of droplets and cleavage. Localized lowering of the surface tension of the droplet may cause a net tension that pulls the droplet toward its center, facilitating splitting but in an uncontrolled manner (Schwartz et al. 2004).

In addition to eliminating surfactants it is possible to enhance uniformity of droplet splitting and dilution through alternative electrode shapes, timing sequences, and the size of the actuation voltages on the electrodes. In the arrangement shown in Fig. 32, three center electrodes are designed to assist in symmetrical droplet alignment prior to splitting. Thus, the three center electrodes are activated initially, which positions the droplet between the two side electrodes. Then these three center electrodes are deactivated and the side electrodes are activated to complete the splitting process (Ren 2004).

In the preparation of a sample for analysis, it is important to concentrate an analyte and remove substances detrimental to that analysis. Purification of DNA has been performed on continuous flow microfluidic devices by flowing samples through silica-based resins or beads (Tian et al. 2000; Wolfe et al. 2002), or through channels with silica-coated pillars (Cady et al. 2004). These solid-phase extraction methods are difficult to use in electrowetting-based devices.

Sample purification has been investigated on EWD devices for the specific application of matrix-assisted laser desorption/ionization mass spectrometry (MALDI-MS) for protein analysis (Moon et al. 2006). In proteomics, sample preparation requires removing unwanted impurities such as salts, non-volatile solvents, and denaturants. Moon et al. have demonstrated sample purification in an air medium by drying a proteomic sample on a EWD device's surface (Fig. 14a), and then rinsing the surface with a water droplet to dissolve and remove hydrophilic impurities. The remaining analyte was then analyzed by MALDI-MS. Thus, the process involved (1) generation of sample droplets, (2) transport and drying of sample droplets on an array, (3) generation of rinsing droplets and transport to the array for washing and selective dissolution, (4) transport and disposal of the wash droplets, and (5) generation of MALDI matrix droplets and transport to the dried array spots (Moon et al. 2006).

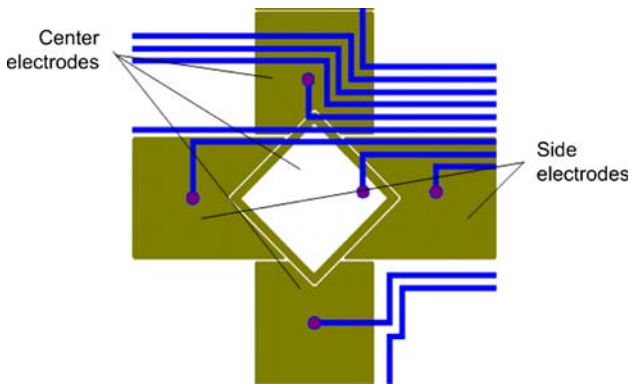

Fig. 32 Electrode shape change to facilitate symmetrical droplet positioning for splitting (Ren 2004)

Sample preparation in EWD devices with a silicone oil medium requires an alternative method to sample drying. One method that has been investigated is the use of magnetic beads with attached analytes or antibodies localized onto the top plate of the device by an external magnet. The beads are then washed with droplets transported to the bead site. This method is described in more detail later. One issue that must be addressed is the fact that the beads will be exposed briefly to the silicone oil between washing droplets. This follows since good washing cannot be achieved by merging a wash droplet with a sample droplet followed by splitting because of rapid mixing of the two droplets. Many such dilution steps are required for sample purification to an acceptable level. Improved results have been achieved by immobilizing the sample and exchanging droplets without droplet coalescence.

With regard to the MALDI-MS application, Srinivasan et al. (2004a, b) demonstrated that a silicone-oil-based EWD device could be used to stamp protein-containing droplets onto a standard stainless steel MALDI plate. Standard sample preparation and purification protocols were performed off chip in a standard well plate. An interface between a well-plate and the electrowetting chip allowed transfer of protein solution into the chip's reservoir. After dispensing from the reservoir, the contents of a protein droplet could be passively stamped onto a target substrate.

By designing the diameter of the stamping hole to be much larger than the spacer thickness (which is also the droplet height), the liquid is passively pushed out of the stamping hole. The larger diameter creates a lower pressure at the stamping hole as compared to the transport layer on the chip, which forces the droplet out spontaneously without active forces (Yi et al. 2003). However, some liquid is still expected to be left behind in the hole as dead volume. And the oil covering the portion of the droplet extending through the stamping hole quickly evaporates if its viscosity is low enough, with the result of oil-free stamping of protein solutions on the receiving plate.

A protein mixture with known constituents (ABI 4700 proteomics analyzer calibration solution) was stamped onto a MALDI plate and the individual proteins were correctly identified in the mass spectrum obtained using MALDI-TOF MS. The preliminary results establish the feasibility of using an electrowetting-based microfluidic system to

handle proteins especially for protein stamping applications (Srinivasan et al. 2004a, b). The experimental set up is shown in Fig. 33.

2.2.2 *Molecular separation*

When mass-limited samples are used in biochemical analysis, it is often required to isolate components that produce a signal of interest so that components can be further processed by amplification, modified, or extracted for identification. Such processes require initial separation followed by fractionation and collection (Ramsey and van Den Berg 2001).

Binary separation and concentration of particles in droplets has been proposed (Cho et al. 2003). The separating procedure involves three steps. First, isolation of each type of particle occurs within the droplet (Fig. 34b) by applying a low-level electric field. The particles can be separated on the basis of their charge and mobility. The second step is to split the mother droplet into two daughter droplets (Fig. 34c). The particles of each charge polarity are more concentrated in one daughter droplet than the other. This step corresponds to the extraction of separated entities. Finally, the third step involves transporting the daughter droplets for subsequent on-chip processing.

The challenges in affecting good particle separation in a droplet according to the method of Fig. 34 are: (1) too low an electric field within the droplet and (2) overcoming internal liquid flow during splitting, which tends to mix the particles. The electric field within the droplet was reported to be 3.3 V/mm (Cho et al. 2003). However, this field is about one order of magnitude less than fields typically used in electrophoretic separation in microfluidic devices: 62.5 V/cm (Tulock et al. 2004); 23.6 V/mm (Lagally et al. 2000); 25 V/mm (Wainright et al. 2003). And with electrophoresis it is possible to separate multiple particles with good resolution based on charge-to-mass ratio and the resulting differing velocities that occur over distances much greater than half a droplet diameter (<1 mm). Thus, the differing particle velocities result in different distances traveled over a given amount of time, rather than simply clumping like particles together in a droplet.

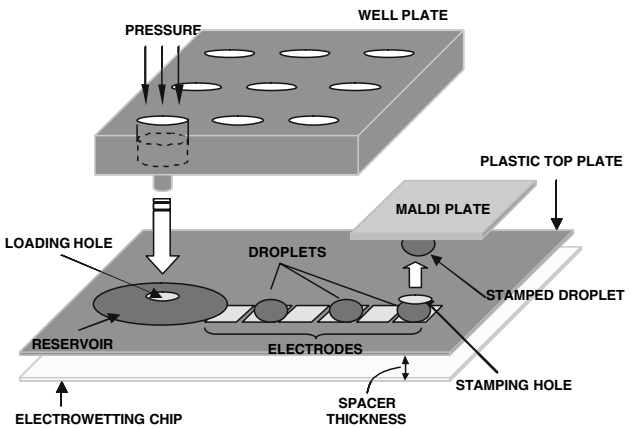

Fig. 33 Schematic view of electrowetting-based protein stamping system. Samples are delivered by pressure from a 96-well plate onto an electrowetting reformatter plate. Droplets are re-routed to the stamping locations and delivered to the MALDI plate by passive stamping (Srinivasan et al. 2004a, b)

To date, there have been no reports of the integration of electrophoresis and electrowetting. The integration would require a digital-to-analog (D/A) interface from the EWD device, where a sample containing DNA, for example, would be presented to the input well of a capillary electrophoresis device for sample injection. An example structure is shown illustrated in Fig. 35. The transfer of the sample droplet to a grounded hydrophilic input well occurs by transferring actuation voltage control to a top electrode placed over the well. The sample introduced into the well is injected by electrokinetic flow, and a plug is formed at the intersection with the separation column running horizontally in Fig. 35. At the end of the separation column the separated DNA is collected at an analog-to-digital (A/D) interface. A droplet is actuated using a top electrode to collect the DNA (insert) followed by dissolution in the droplet and subsequent transport. This scheme addresses the need to separate the low voltage power supply used for electrowetting from the high voltage power supplies used in capillary electrophoresis (Vijay et al. 2006).

Separation in an EWD device using magnetic beads is also possible. Magnetic beads coated with antibodies have been successfully used to concentrate a variety of microorganisms from dilute environments. An immuno-magnetic assay consists of attaching the required antibody to a magnetic bead in the sample solution. The bead-carrying droplet can be transported to a region of the device with a magnet placed on the top plate. Magnetic beads coated with the antibody of interest can be confined to a single electrode via a concentrated magnetic field, while the solution surrounding the beads can be exchanged with a new solution (reagent-containing or washing solution) via a simple droplet merging and splitting routine. This scheme is illustrated in Fig. 36 for the example of separating a pathogenic target with a magnetic bead having attached antibodies.

The ability to manipulate magnetic microspheres in solution on a EWD device will expand the variety of tasks that can be performed if the microspheres are used as analyte immobilization surfaces. Because the microspheres can be transported in solution and immobilized by a magnetic field, the use of microspheres on-chip will not alter the reconfigurability or reusability of the chip. The retention of 8 μm diameter magnetic microspheres during

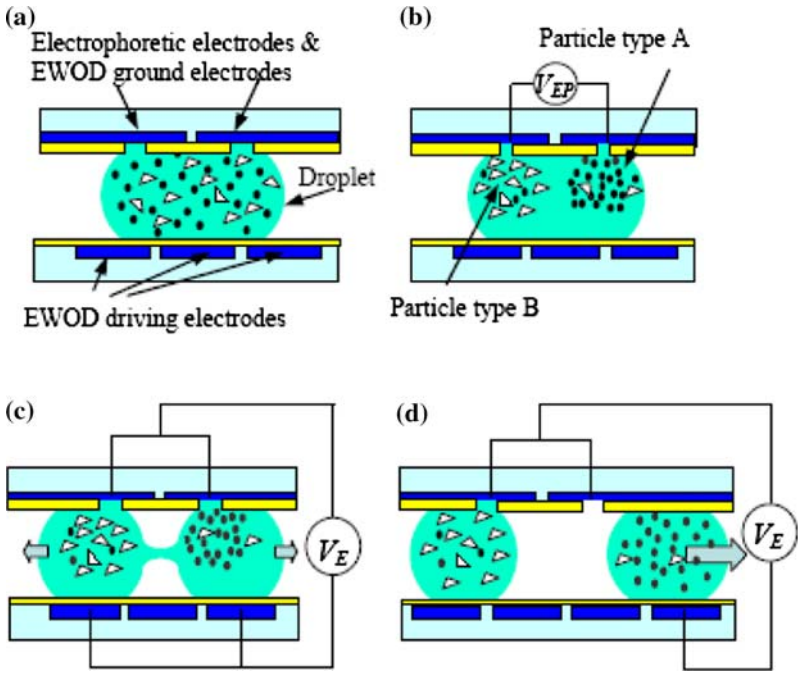

Fig. 34 Binary particle separation within a droplet. **a** Droplet with particle type A and B; **b** charge separation within the droplet; **c** droplet splitting; **d** transport of split daughter droplets (Cho et al. 2003)

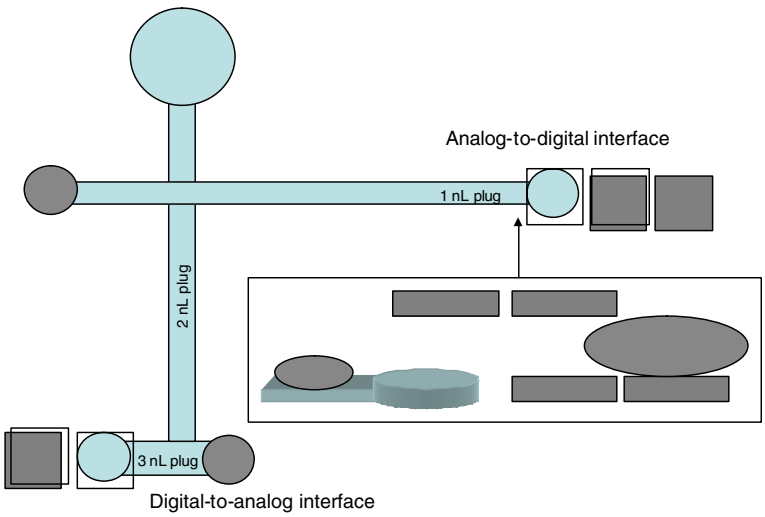

Fig. 35 Proposed interface between electrowetting and capillary electrophoresis (Vijay et al. 2006)

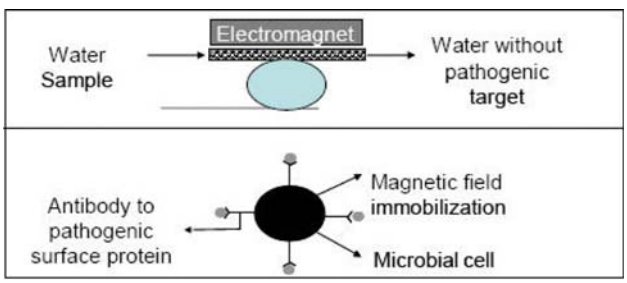

Fig. 36 Attachment of a pathogenic target to antibodies on a magnetic bead, immobilization of the beads by a magnet on the top plate, followed by bead washing by droplet transfer over the immobilized beads

droplet splitting has been demonstrated on a digital microfluidic platform. A droplet of deionized water was merged with a droplet containing magnetic microspheres, and Neodymium-–Iron-–Boron magnets were placed on the cover plate of the EWD chip. When the combined droplet was split, the magnetic microspheres were isolated in the daughter droplet in closest proximity to the magnets (Fair et al. 2005).

As noted above, magnetic beads coated with the DNA samples of interest can be confined to a single electrode via a concentrated magnetic field, while the solution surrounding the beads can be exchanged with a new solution

(reagent-containing or wash solution) via a simple droplet merging and splitting routine. This not only allows for chip reusability, but also eliminates the need for surface chemistry. However, early experiments with magnetic beads have shown less than 100% bead retention after washing (Fair et al. 2005). Imperfect bead retention results in sample loss as well as platform contamination. The problem seems to be that some beads are washed away by droplets as the droplets pass over the magnetized beads. This result may be due to poor magnetic properties of some beads, the solubility of the beads in the droplet's liquid, or the surface tension force exerted on the beads by the droplet's meniscus.

The percent retention rate of magnetized beads was measured after sequential washing of a 100 droplet sequence. A 150 μm thick micro cover glass was used as the top plate. It was spin coated with Teflon AF to create a hydrophobic surface. An N-50 grade cylinder magnet (1.5 mm diameter, 5 mm long) was then attached to the non-Teflon side of the top plate. About 1.5 μL of Dynabeads MyOne Streptavidin T1 (~7–12 $\times$ $10^6/\mu$L) magnetic beads were pipetted onto the Teflon-coated side of the top plate directly opposite the magnet. The top plate system was then placed under a digital video camera. The top plate was placed on spacers to get a tilt of about 10°. About 50 μL droplets of DI water were pipetted onto the top plate above the beads and allowed to slide down the Teflon-coated top plate and wash over the magnetic bead area. This process was repeated 100 times to obtain a drop by drop, time-dependent profile of the magnetic bead retention. Image analysis was performed to compare the number of pixels between frames to determine the percentage of magnetic beads remaining. The results are posted in Fig. 37 in a scatter plot showing the overall percent retention after each drop compared to the initial magnetic bead count. The results show that about 51% of the magnetic beads remain on the top plate after 100 washes. The majority of beads were lost with the washing of the first droplet. The most significant result is that after about 20 washes the rate of bead loss goes almost to zero (Fitzpatrick 2006). This result was verified in experiments performed on an electrowetting chip, where the percentage of retained beads was about 60% after 20 washes with no further loss. Thus, pre-washing beads with buffer droplets would prepare the top plate for reproducible on-chip assays.

2.2.3 *Assays*

On-chip assays for determining the concentrations of target analytes is a natural application for digital microfluidics (Srinivasan et al. 2003a, b, 2004a, b; Aizenberg et al. 2006; Jary et al. 2006). The specific focus of work in this area has been on multiplexed assays, where multiple analytes can be measured in a single sample. The on-chip process steps include the following: (1) pre-diluted sample and reagent loading into on-chip reservoirs; (2) droplet dispensing of analyte solutions and reagents; (3) droplet transport; (4) mixing of analyte solution and reagent droplets; and (5) reaction product detection. The compatibility of each chemical substance with the electrowetting platform must be determined initially. Compatibility issues include the following: (1) does the liquid's viscosity and surface tension allow for droplet dispensing and transport by electrowetting? (2) Will the contents of the droplet foul the hydrophobic surfaces of the chip? (3) In systems with a silicone oil medium, will the chemicals in the droplet cross the droplet/oil interface, thus reducing the content in the droplet? Three examples of assays that have been performed successfully on digital microfluidic platforms include glucose, nitroaromatic compounds, and air-borne inorganics.

The in vitro measurement of glucose in human physiological fluids is of great importance in clinical diagnosis of metabolic disorders. Srinivasan et al. (2004a, b) have demonstrated a colorimetric enzyme-kinetic method based on the Trinder's (1969) reaction used for the determination of glucose concentration. The on-chip glucose assay was performed in three steps—dispensing of samples and reagents from on-chip reservoirs, mixing and detection.

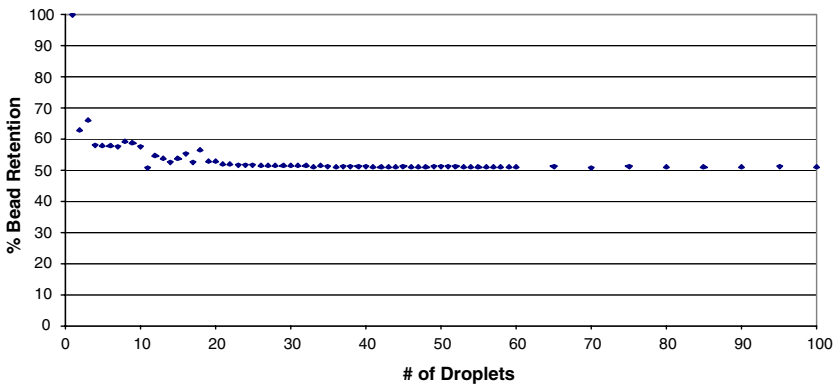

Fig. 37 Magnetic bead retention after droplet washing. *Vertical scale*: % bead retention; *horizontal scale*: number of wash droplets. Fifty percent retention remained constant at 20 drops

Three different glucose samples were assayed three times each (nine sequential assays) to evaluate within-run variation. Three different concentrations of glucose (40, 80, and 120 mg/dL) were assayed three times each in a serial fashion. The absorbance was measured using a 545 nm LED photodiode setup as a function of time for the nine assays is shown below in Fig. 38 along with an image of the chip used in the experiments (Srinivasan 2005). The variation was less than 3% which indicates excellent droplet volume reproducibility with no detectable carry-over.

Perhaps, the most critical step in performing an assay is dispensing analytes and reagents from the on-chip reservoirs. The process of forming a droplet can be significantly affected by the solution content, particularly if protein solutions are used. The issue appears to be protein absorption in the liquid reservoirs, which have a much larger surface area than the electrodes (Srinivasan et al. 2004a, b). Dilution of sample volumes is also an important step in almost all bio-analytical systems to reduce the effect of interfering substances and to increase the linear range of operation of devices. Issues in dilution have been discussed above.

Preliminary results have been obtained from detecting commercial grade 2,4,6-trinitrotoluene (TNT) and pure 2,4-dinitrotoluene (Pamula et al. 2005a, b). Assays were performed on an electrowetting chip in three steps: dispensing, mixing, and colorimetric detection. Nitroaromatic compounds such as TNT/DNT react with nucleophiles (bases) such as hydroxides and alkoxides, to form colored Jackson–Meisenheimer complexes. Acetone, acetonitrile, and methanol have been the most popular solvent choices for TNT analysis, even though this reaction has been demonstrated in various organic solvents. All these three solvents are currently incompatible with oil-medium electrowetting systems, since they are miscible with silicone oil. DMSO is another versatile solvent which dissolves most aromatic hydrocarbons, including nitroaromatics such as TNT, and yet is immiscible with silicone oil, making it compatible with the electrowetting platform. DMSO is also completely miscible in all proportions with water and has a low order of toxicity. For these reasons DMSO was chosen as the solvent to develop the TNT reactions. DMSO is also known to enhance the stability of the Jackson–Meisenheimer complex (Terrier 1982).

Another example of an assay developed on a digital microfluidic platform is one that relies on the use of a solvent. Initially, it was determined by Pollack (2001) that the low viscosity silicone oil used as a medium on electrowetting chips was found to mix with many solvents, including ethanol and methanol. However, solvent-based assays can be developed that are compatible with the oil-based platform. The application is atmospheric sampling of sulfate particles.

Knowledge of aerosol composition as a function of size is critical for understanding the origin, properties, and health effects of particulate matter. Size-segregated chemical composition of aerosol is usually measured using cascade impactors, such as Micro-Orifice Uniform Deposit Impactors (MOUDI, MSP Inc.). In cascade impactors aerosol is collected on several stages with progressively smaller cut-off diameters. The aerosol is impacted on aluminum or Teflon filter substrates, which after collections are washed in ultra-pure water and the extract is analyzed. Because each of the preparation, sampling, and analysis steps is manual, impactors require a large amount

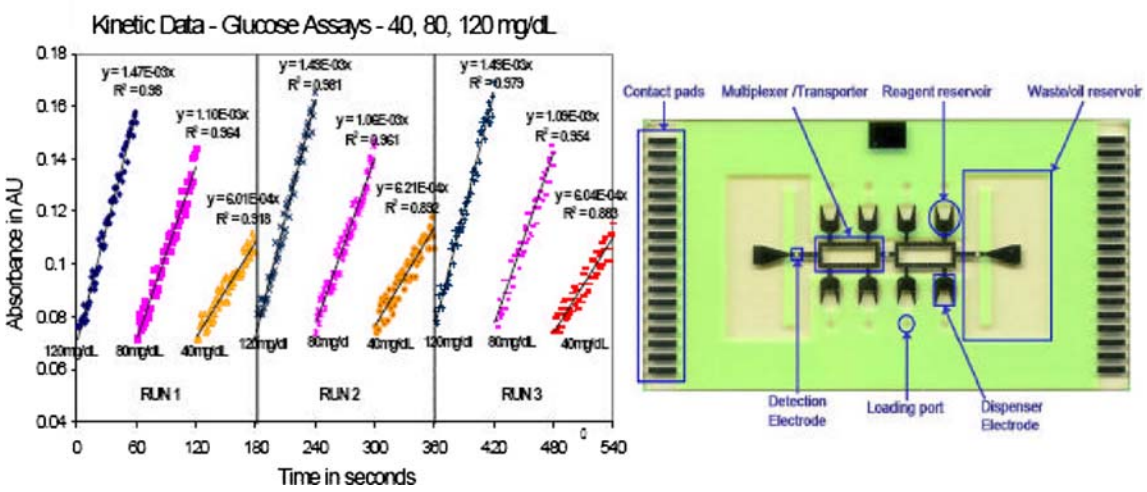

Fig. 38 Nine fully automated glucose assays performed in succession by dispensing droplets of reagent and droplets of one of the three different glucose standards (40, 80, and 120 mg/dl), mixing the droplets and transporting the reactants to a detector. The absorbance time course for the experiment (*left*) and the chip photo (*right*) (Srinivasan 2005)

of manual handling to obtain one sample, which makes their application extremely expensive.

Automated on-chip measurement of airborne particulate matter has been proposed using a scanning droplet method (Fair et al. 2004; Zhao and Cho 2006). Sample collection is performed by impacting airborne analyte particles directly onto the surface of the electrowetting chip. After the collection phase, the surface of the chip is washed with a micro-droplet of solution. The droplet is digitally directed across the impaction surface, dissolving sample constituents. Because of the very small droplet volume used for extraction of the sample from a wide collection area, the resulting solution is relatively concentrated, and the analyte can be detected after a very short sampling time (1 min) due to such pre-concentration. After the washing phase, the droplet is mixed with specific reagents that produce colored reaction products. The concentration of the analyte is quantitatively determined by measuring absorption at target wavelengths using a simple light-emitting diode and photodiode setup. Target applications include quasi real time sampling of airborne contaminants and bioagents, and detection and quantification of nitroaromatic explosive particles.

Recent work (Ma et al. 2006, unpublished) has been aimed at implementing the methyl-thymol blue (MTB) method for sulfate determination (Mudsen and Murphy 1981). Sulfate is the major aerosol component in the atmosphere, comprising 30–80% of the fine aerosol mass (Seinfeld and Pandis 1998). Colorimetric detection of sulfate was used and was based on the traditional method by Mudsen and Murphy (1981) with some modifications to the reagent composition. Ethanol is the traditional reagent solvent; however, it proved incompatible with the digital microfluidic platform due to its solubility in the silicone oil. After testing several alternative solvents, the best results were obtained with 40% methanol. Measurements of absorbance at 608 nm were used for sulfate detection. Measurements showed a linear relationship for sulfate concentration ranging from the limit of detection of 0.5–150 mg/L (Ma et al. 2006, unpublished).

Droplet scanning and sample collection must be performed in air without a top plate, so as not to perturb impactor air flow. To prevent evaporation, the scanning droplet can be clad with its own oil encasement, which surrounds the droplet and travels in air with the actuated droplet. This oil cladding has been demonstrated by transporting the droplet through the interface between the oil medium and the air (Fair et al. 2004). Once sample collection is complete, the collection droplet must be moved through an air/oil interface into the analytical section of the LoC. The design and reliability of an appropriate oil/air interface system on chip has not yet been demonstrated.

The integration of optical detectors is relatively easy to perform on a digital microfluidic platform, especially since the platform is made using plates and see-through indium-–tin-–oxide electrodes. However, optical absorbtion detection scales poorly with miniaturization, since Beer's law incorporates a pathlength dependence (Madou and Cubicciotti 2003). Regarding the detectors reported by Srinivasan et al. (2004a, b) the optical path length typically is 100–300 μm, which is 30–00 times smaller than conventional systems (10 mm). This small path length poses serious sensitivity issues.

2.2.4 PCR

Polymerase chain reaction (PCR) is a method for creating copies of a specific portion of a DNA molecule to produce large quantities of DNA for biochemical analysis. Since the first report of specific DNA amplification using the polymerase chain reaction (PCR) in 1985 (Stryer 1995), PCR has become a powerful tool for most areas in biology. It is used in genotyping, sequencing, expression analysis, diagnostics, and many other areas of modern biology and medicine.

PCR involves the exponential amplification of small fragments of DNA. It is based upon a doubling of the concentration of a certain segment of double-stranded DNA during a single thermal cycle. If n thermal cycles are performed, then the DNA amplification factor is 2^n. The method uses repeated temperature cycling of DNA samples using three different temperatures to achieve amplifications of up to 10^9. A conventional PCR thermal cycle consists of three steps:

1. Strand separation: The two strands of the parent DNA molecule are separated by heating the solution to 95°C for 45 s.
2. Hybridization of primers: The solution is then abruptly cooled to 54°C to allow each primer to hybridize to a DNA strand. This annealing process takes 30 s.
3. DNA synthesis: The solution is then heated to 72°C, the optimal temperature for *Taq*DNA polymerase. This allows the *Taq*DNA polymerase to attach at each priming site and extend a new DNA strand. The process takes 90 s.

Today, PCR is usually performed in large thermocycler systems that heat/cool 96, 384, or 1,536 assay well plates. Each well in a plate must be robotically loaded/unloaded with a sample compound in multiple-step processes that use micro-dispensing technology based on either syringe pump-based pipettors or peristaltic pumps. Typically, such micro-dispensing is limited to 3–5 μl volumes due to evaporation during handling and difficulties in small volume handling (Nakane et al. 2001).

One key to lowering the cost of sequencing is to use scalable chip technology with new architecture that allows automated sample preparation, sample handling, sample analysis, and much smaller sample volumes to enhance the throughput of gene sequencing by significant factors. While numerous studies of on-chip PCR have been reported on continuous-flow microfluidic chips (Lagally et al. 2000; Schneegass et al. 2001; Cady et al. 2004; Ottesen et al. 2006), much less work has been reported on electrowetting or electrostatic-based PCR devices (Tokoro et al. 2002; Pollack et al. 2003; Fair et al. 2003). Nevertheless, the advantages of performing PCR using droplet-based electrowetting over continuous flow PCR have been analyzed, and it was demonstrated through simulation that droplet-based PCR provides higher performance and lower design and integration complexity. (Zhang et al. 2004).

PCR using droplets in miniemulsions has been reported (Musyanovych et al. 2005), and Wang et al. (2005) have described a droplet-based oscillating-flow PCR chip made using a silicon microfabrication method. These studies and others have demonstrated the viability of droplet-based PCR in performing the required steps of denaturation, annealing, and extension processes.

The key advantages of using droplets for performing PCR are (1) the ability to use smaller volumes of reagents, thereby reducing reagent costs by orders of magnitude; (2) faster thermal cycle times with smaller thermal mass; (3) the potential for automation to link PCR with on-chip separation and detection; (4) fewer human errors; and (5) parallel sample processing.

To evaluate the suitability of electrowetting-based PCR, it was necessary to address the following questions: (1) Are the PCR reagents compatible with electrowetting? (2) What is the effect of electrowetting on PCR? (3) Is electrowetting compatible with the high temperatures required by PCR? and (4) is Is cross-contamination an issue?

To address the issue of reagent compatibility, Pollack et al. (2003) studied electrowetting transport of droplets containing a pre-PCR ‘‘mix’’. The ‘‘mix’’ contained 1 µl of template DNA, 2 µl of dNTPs, 2 µl of forward primer, 2 µl of reverse primer, 2 µl of buffer (1.5 mM $MgCl_2$), 1 µl of the enzyme Taq Polymerase, and 10 µl of water. A droplet of 900 nl was pipetted onto the electrowetting chip and transported at 30 V. The droplet was transported back and forth over four electrodes for about 0.5 h, which amounted for around 2,000 transfers. PCR was then performed in a conventional thermocycler on a fresh sample taken from the same pre-PCR mix as described above. After amplification, it was possible to transport the post-PCR mix as easily as the pre-PCR mix. These results showed that electrowetting transport of droplets before PCR and after PCR amplification is not affected by the enzymes present in the PCR mixtures.

The effect of electrowetting on PCR was also addressed. Alter PCR of the pre-PCR mix, noted above, the sample was then cycled in a conventional thermocycler. The sample was then loaded into an agarose gel for electrophoresis. A strong band was observed with comparable intensity to a control sample, demonstrating that electrowetting actuation had not inhibited PCR amplification (Pollack et al. 2003).

With regard to thermal cycling effects on electrowetting, Pollack et al. (2003) also performed PCR on an EWD chip using a hot-air thermocycler that heated the entire chip. The EWD chip contained four loading ports and a single line of four electrodes extending from each port. The entire chip was placed in a chamber through which heated air was circulated. A thermocouple placed directly inside the chip provided feedback for proportional integral-derivative (PID) control of the heaters and fans and heating/cooling rates faster than 1°C/s and stability to within ±0.5°C were achieved. The entire assembly including the hot-air thermocycler and chip was mounted on the stage of an inverted fluorescence microscope to permit real-time fluorescence observation of the droplets contained inside.

As the temperature of the chip was increased during thermocycling, the electrowetting threshold voltage decreased, allowing for faster velocity of the transported droplet. Figure 39 shows the threshold voltage as a function of chip temperature (Pollack et al. 2003). The voltage reported here is that which is measured to oscillate a 1.7 µl droplet at 5 Hz over four electrodes. The data shows that the voltage required to maintain the oscillation of the droplet at 5 Hz decreased with increasing temperature. Conversely, at a fixed voltage and increasing temperature, the droplet moved faster. The threshold voltage was reduced by as much as 30% for a 50°C increase in temperature. This beneficial result will allow faster droplet transport through the heater zones during PCR.

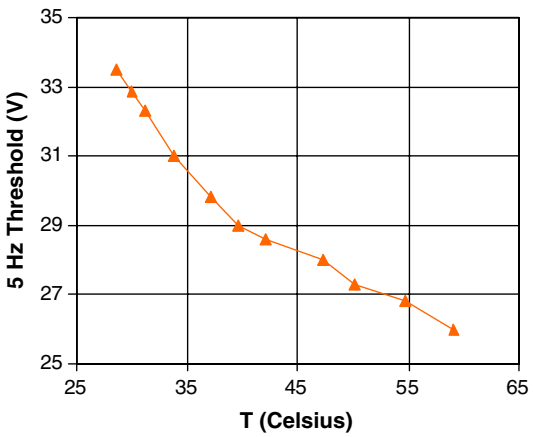

Fig. 39 Temperature dependence of the threshold voltage for electrowetting droplet transport (Pollack et al. 2003)

It also was observed that at temperatures close to 100°C a droplet starts evaporating from the electrowetting chip. In Pollack's experiments, silicone oil was used as a filler fluid that surrounded the droplets. This significantly slowed droplet evaporation, allowing for the use of much smaller volumes than conventional systems. During thermal cycling the maximum droplet temperature was 94°C. To get a preliminary assessment of droplet-based thermocycling, a heating experiment was performed with a cytoplasmic beta-actin gene with molecular beacon probes attached to it. When the sample was heated with an integrated thin film heater on an electrowetting chip, fluorescence was observed from the molecular beacons within 3 s, which showed that the DNA had denatured! No loss of droplet volume was observed. This result demonstrated that strand separation in a 1 µl droplet sample can be performed in 3 s rather than 45 s required in conventional systems (Pollack et al. 2003; Fair et al. 2003).

It is expected that in a high-throughput system, droplets containing different PCR samples may have to be routed over common sets of electrodes on the chip. Thus, cross-contamination between droplets must be considered. Adsorption of DNA to silicon-glass chips is a big problem faced by the PCR community, and there are many ways of passivating the surface to reduce adsorption (Shoffner et al. 1996).

Carry-over between droplets during electrowetting transport was evaluated by alternately transporting DNA-containing and DNA-free droplets across a series of common electrodes to determine whether DNA could be transferred between the two droplets. The DNA-containing droplet was 2.0 µl of allele to control solution and the DNA-free droplet was 2.0 µl of Tris-EDTA buffer. The two droplets were programmed to oscillate simultaneously back-and-forth across the five closest electrodes with a three electrode separation maintained between the droplets at all times (Fig. 40). Since the middle two electrodes were included in the flow paths of both droplets, there was an opportunity for each cycle to transfer DNA from the DNA-containing to the DNA-free droplet through contamination of the chip surfaces. The intersecting flow protocol was run for 5,000 complete cycles at a droplet transfer rate of 16 Hz at 55 V dc. Thus, each droplet was transferred 40,000 times during the course of the 45 min experiment, with 15,000 of those transfers occurring on shared electrodes. Each of the droplets were then extracted from the chip and added to a DNA-free PCR cocktail. Along with a control consisting of 2 µl of allele to control solution transferred directly from a silicone-oil-containing Eppendorf tube to the PCR cocktail mixture, the samples were amplified in commercial real-time thermocycler (Cepheid Smartcycler). The results shown in Fig. 40 indicate that there was no substantial cross-contamination between the droplets (Fair et al. 2003).

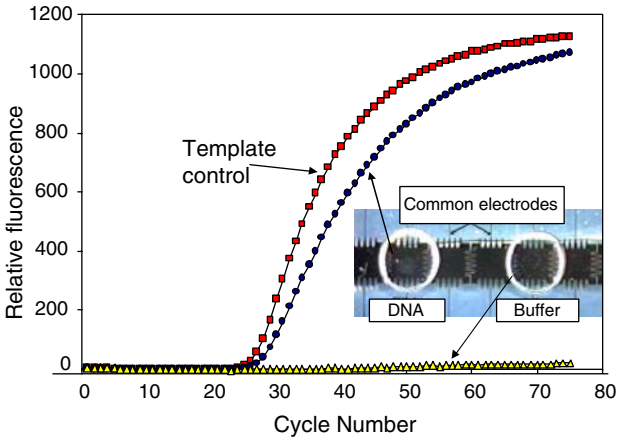

Fig. 40 Carry-over between droplets during electrowetting transport was evaluated by alternately transporting DNA-containing and DNA-free droplets across a series of common electrodes (see *insert*) to determine whether DNA could be transferred between the two droplets. Each of the droplets were then extracted and added to a DNA-free PCR cocktail. Along with a control the samples were amplified in commercial real-time thermocycler (Cepheid Smartcycler) (Pollack et al. 2003)

Typical amplification time-courses for both the conventional thermocycler and an electrowetting system are shown and compared in Fig. 41. In both cases, amplification of DNA is evident as the fluorescent signal rises above the background level between the 20th and 30th cycles (Pollack et al. 2003).

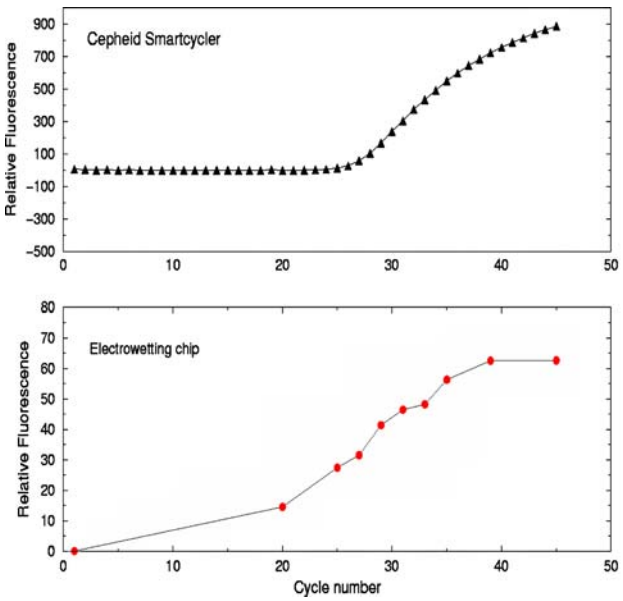

Fig. 41 Typical amplification time-courses for both the conventional thermocycler and an electrowetting system showing relative fluorescence versus cycle number (Pollack et al. 2003)

2.2.5 *Sequencing of DNA*

The number of bases in Genbank has increased exponentially with a doubling period of approximately 18 months and currently contains about 3×10^{10} bases, equivalent to the content of ten human genomes. In 10 years time, the database will contain the equivalent of approximately 1,000 human genomes and in 20 years it will contain the equivalent of 100,000 human genomes. Achieving the productivity necessary for the continued exponential growth of sequence information will require new methods for sequencing that are intrinsically scalable and contain no inherent limit on their operation.

There are several competing technologies that propose the use of microfluidic technologies to reduce reagent costs, which have emerged as the primary cost of Sanger-based sequencing along with the instrument cost. These technologies include mass spectrometry (Jurinke and van den Boom 2002), nanopore sequencing (Deamer and Akeson 2000; Deamer and Branton 2002; Li and Gershow 2003), sequencing-by-hybridization (Bains and Smith 1988; Fodor et al. 1995; Drmanac 1998; Brenner et al. 2000), sequencing-by-synthesis (Metzger at al. 1994; Kartalov and Quake 2004), single-molecule sequencing methods (Braslavsky et al. 2003; Mitra et al. 2003), miniaturized electrophoretic methods (Koutny et al. 2000; Emrich 2002; Paegel et al. 2003), and miniaturized pyrosequencing (Margulies et al. 2005).

Work currently is underway to evaluate the EWD microfluidic platform to perform miniaturized sequencing by synthesis. Sequencing-by-synthesis methods involve enzymatic extension by polymerase through the iterative addition of labeled nucleotides, often in an array format. The cascade begins with the addition of a known nucleotide to the DNA (or RNA) strand of interest. This reaction is carried out by DNA polymerase. Upon nucleotide incorporation, pyrophosphate (PPi) is released. This pyrophosphate is converted to ATP by the enzyme ATP sulfurylase. The ATP then provides energy for the enzyme lucerifase to oxidize luciferin. One of the byproducts of this final oxidation reaction is light at approximately 560 nm. This sequence is illustrated in Fig. 42. The light can be easily detected by a photodiode, photomultiplier tube, or a charge-coupled device (CCD) camera. Since the order in which the nucleotide addition occurs is known, one can determine the sequence of the unknown strand by formation of its complimentary strand. The entire pyrosequencing cascade takes about 3–4 s from start to finish per nucleotide added (Ronaghi 2001).

A prelimary example of a digital microfluidic pyrosequencing platform is shown in Fig. 43 (Fair et al. 2007). The chip has reservoirs to house nucleotides and enzymes. The pyrosequencing protocol can be easily integrated onto

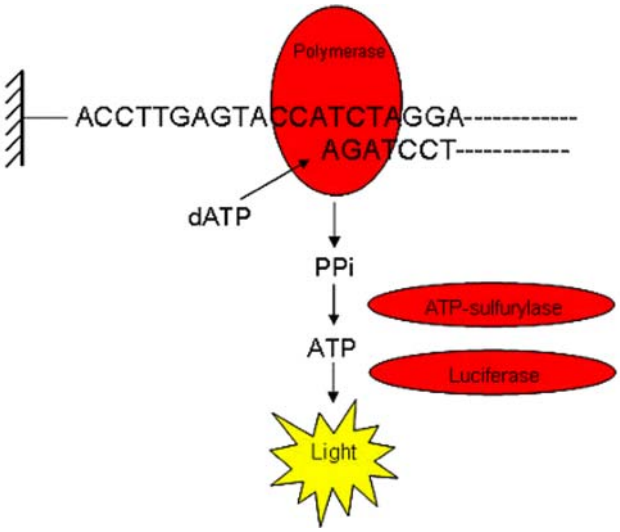

Fig. 42 Illustration of solid-phase pyrosequencing. After incorporation of a nucleotide (in this case dATP), a washing step is used to remove the excess substrate

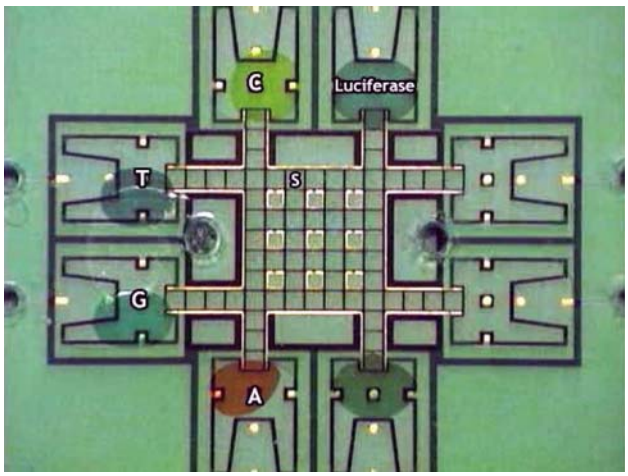

Fig. 43 Prototype pyrosequencing chip from advanced liquid logic with on-chip reservoirs for dispensing reagents and nucleotides A, T, C, and G. The DNA is attached to the ''S'' sample location indicated on the photo (Fair et al. 2007)

such a system. The on-chip chain of events is as follows: (1) a droplet containing nucleotides of a single type (and polymerase) is dispensed from the reservoir and brought to site ''*S*,'' which contains immobilized single-stranded DNA, (2) the droplet is allowed to incubate, allowing time for polymerization to take place, (3) the droplet is removed from site ''*S*'' and allowed to react with luciferase, and (4) the lucerifase-containing droplet is sent to a detector array (not shown in the diagram). While the detector array works to detect a light signal from the droplet, the next nucleotide-containing droplet is brought to site ''*S*,'' allowing DNA synthesis to occur simultaneously with detection. This protocol allows for optimized synthesis reactions to

take place, and because synthesis is physically separated from detection, this system has potentially no inherent limitation on its read length.

The significance of separating the synthesis and detection can be especially appreciated since this method allows feedback control of the nucelotide additions to the reaction site at the optimum time. The light output can be monitored in real time, and if excess light beyond what is expected for a single nucelotide incorporation event is detected, then additional nucelotides and additional reaction time can be programmed to extend and fully incorporate a homopolymer run. Also, the timescales for synthesis and detection are different, so independent optimization of each step is permitted.

One of the chief requirements for performing pyrosequencing on an electrowetting chip platform is DNA immobilization via surface attachment. While DNA is commonly tethered to glass and silica substrates for various biochip and microarray applications, the EWD microfluidic platform is coated with a relatively inert, hydrophobic Teflon thin film, posing a challenge for surface modification and surface chemistry.

On-chip DNA immobilization has been shown to be feasible with gold particles, although droplet transport over the gold particles dislodges them. A better method is the use of streptavidin, which binds well to aminosilane and glutaraldehyde-treated glass top plates. This method requires patterning of the Teflon film to create small access windows to the treated glass surface. Furthermore, unlike adherence of gold to the Teflon surface, which is non-covalent, streptavidin binds covalently to the surface, ensuring that the protein will remain attached after droplet transport. Additionally, biotinylated DNA is guaranteed to bind well to streptavidin because streptavidin has an extremely high affinity for biotin ($K_a \sim 10^{13}\,M^{-1}$). Further, commercial pyrosequencing relies on the use of a streptavidin substrate to bind biotinylated DNA (Ronaghi 2001). This being the case, it is likely that the reagents used for pyrosequencing will not hinder the streptavidin–biotin interaction. To date, however, the most successful and versatile approach to binding DNA on the EWD platform has been through magnetic bead attachment, as discussed above.

Specific issues regarding the compatibility of droplet-based electrowetting with pyrosequencing are (1) Are the reagents compatible with electrowetting? (2) What is the effect of electrowetting on pyrosequencing? (3) Are synthesis reactions scalable for parallel processing? (4) What is the effect of DNA exposure to the silicone oil medium on chip?

With regard to (1), it has been verified that 1 μl droplets of ATP assay reagent and 1 μl droplets of variable ATP solution concentration produce a linear response in a photomultiplier (PMT) detector as a function of ATP concentration down to femtomolar concentrations (Pollack et al. 2006). It has also been verified that mixing 1 μl droplets of APS/sulfurylase with 1 μl droplets of variable concentrations of PPi produced a linear PMT response up to 2 pmols of PPi (Pollack et al. 2006).

With regard to the scalability of synthesis reactions, there are basic scientific and engineering issues that must be addressed in the scaling of an electrowetting-based microfluidic platform to picoliter droplets. The impact of scaling droplet volumes by a factor of 1,000–1,000,000 from the current scale translates to linear dimension scaling of electrode pitches from hundreds of microns to 10 μm and switching times of electrode potentials from 50 up to 10 kHz. Such scaling is critical to massively parallel on-chip DNA sequencing at high clock rates. Thus, sequencing of a 1 Mbp-long genome would require 1,000 parallel sequencing channels at 1,000 bp reads/channel.

3 Lab-on-a-chip system integration

In the sections above, the work on developing a digital microfluidics toolkit has been review. The application of this toolkit containing electrowetting-based microfluidic operations for performing fluidic functions has been discussed. The question, however, still remains: Can digital microfluidics deliver a true lab-on-a-chip technology that is adaptable to numerous applications? The answer to this question is still out, but each fall semester this author is privileged to teach a graduate course at Duke University entitled *Biochip Engineering*. The students come from biomedical engineering, electrical engineering, chemistry, and mechanical engineering departments at Duke. And, they have no built-in biases regarding microfluidics and technology choices! They are assembled into multidisciplinary design teams and asked to identify an application for a lab-on-a-chip and to choose *any* microfluidic technology that will enable that application to be performed in a miniature format. The course reviews the entire microfluidic technology arsenal, and half way through the semester the students must have developed the chip architecture and have chosen a technology for implementation. So far, all of these design teams have chosen to implement at least a portion of their devices in droplet-based electrowetting technology. Two example applications and chip architectures from this class are described below, which underscore the versatility of EWD devices in implementing fluidic functions.

3.1 Analog/digital hybrid microfluidic chip for DNA and RNA analysis

The first application is an analog/digital hybrid biochip that performs multiple biomedical functions on a blood sample,

including DNA detection and real-time PCR analysis (Pan et al. 2006). The chip benefits from the advantages of continuous microfluidics for sample preparation and reagent delivery and discrete microfluidics for reconfigurable microanalysis.

The hybrid microfluidic chip contains three main units: the Sample Preparation Unit (SPU), the Digital Microfluidic Workshop (DMW), and the Reagent Cartridge (RC). The SPU uses a continuous (analog) microfluidic technology to perform DNA/RNA extraction from raw blood samples. The RC is the external supplier of the biological reagents and detection probes, and it also uses continuous flow technology. The DMW serves as the core biomedical analysis unit, and it adopts the droplet-based (digital) microfluidics technique. As shown in Fig. 44, the SPU and RC are connected to the DMW through separate I/O interfaces to form a self-contained biomedical analysis system (Pan et al. 2006).

The architecture in Fig. 44 is based on the MONARCH architecture, which segments sections of a microfluidic chip into specific fluidic functions and connects these sections with transport buses (Jopling 2001). The SPU unit is designed based on previous work by Liu et al. (2004). Due to the difficulty of performing mixing on the SPU chip, mixing of the blood sample with lysis buffer and chaotropic salt is performed before loading the sample to the chip. The SPU performs the remaining DNA extraction and purification. The blood sample is loaded into the SPU. The blood cells have to be separated before cell lysis can be performed. DNA/RNA extraction and purification are then carried out in a continuous flow format. The output of the SPU is purified DNA/RNA solution, which is then transported to the DMW.

The interface to the DMW chip is performed via a single port that loads an on-chip reservoir. A special reservoir is required for transition from typical values of 50–100 μl in the analog technology to about 30 nl in the electrowetting technology. The DMW receives the purified DNA/RNA solution from the SPU and the reagents from the RC. In order to perform the required biological assays, it is necessary to convert the continuous fluid into discrete droplets that will be submerged in a silicone oil medium. The basic functional components of the DMW include mixers, reservoirs, temperature controllers, and detection units as shown in Fig. 44. All of these components are independent of each other. The droplets are moved into the desired components through a multi-channel transportation bus and are controlled by an external computer processor. The DMW is the core analytical device and is the only unit that is reusable and reconfigurable (Pan et al. 2006).

The fluidic architecture of DMW is illustrated in Fig. 45. The SPU and RC are connected to the A/D converter, where the continuous flow is converted into digital droplets. The droplets are then transported through the I/O bus to the various addressable buffer zones. This procedure takes place at the beginning of each experiment. The buffer zone resembles the function of RAM memory in a personal computer. The buffer zone holds all the chemicals and samples required in the experiments, thus avoiding speed bottlenecking at the A/D converter (Pan et al. 2006).

As shown in Fig. 45, all the components are connected to the main transportation bus. Using the transportation bus, the droplets move through different zones such as mixing and reaction. The temperature control (TC) zones are the regions with protocol-defined temperatures maintained by electrical heaters and temperature sensors. Since most reactions have optimal temperatures, the TC zones are critical for biological assays. Due to the fact that PCR analysis usually requires at least three different temperatures, three TC zones are built in the chip. TC zones are connected to each other by their own transportation channels, and PCR can be easily carried out by shuttling droplets back and forth. An optical monitoring unit is incorporated in one of the TC zones for fluorescent signal detection in real-time PCR.

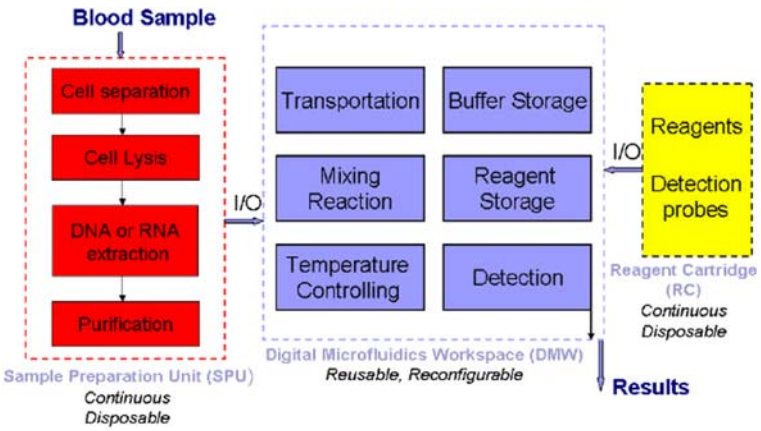

Fig. 44 Top-level architecture of an analog/digital hybrid biochip that performs multiple biomedical functions on a blood sample, including DNA detection and real-time PCR analysis (Pan et al. 2006)

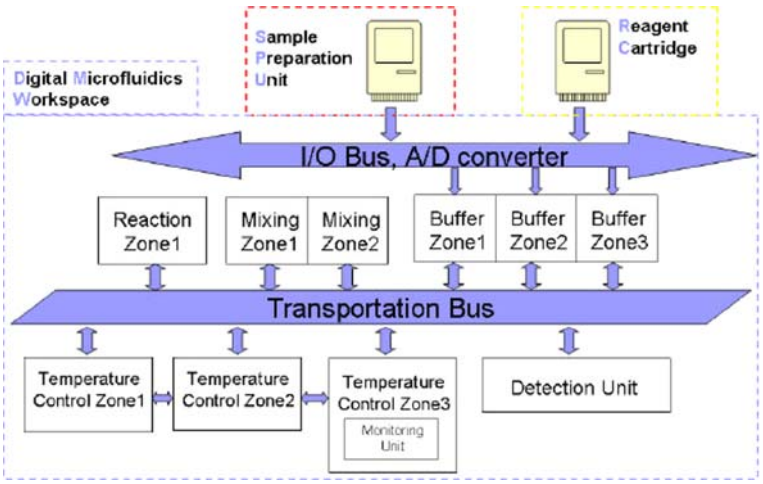

Fig. 45 The fluidic architecture of Digital Microfluidic Workspace (Pan et al. 2006)

The floorplan of the DMW is shown in Fig. 46 (Pan et al. 2006). There are a total of seven ports (represented by the circles in the floor plan design) connecting the DMW unit with other units or outside systems. The sample input port is designed to integrate the DMW unit and continuous flow based SPU unit. The four reagent buffers are connected to the RC unit. The fluid is dispensed as droplets and saved in corresponding I/O buffer zones. A washing buffer port is connected to the I/O transportation bus. In addition, a washing buffer port and a waste port are connected to a central transportation bus.

The central transportation bus is a dual-channel bus connected to all the components on the chip. Buffer zones store droplets needed in each experiment. Two mixing/reaction zones can perform six mixing operations in parallel. Three temperature control zones are placed on the other side of the central bus. They are connected to each other by a bus called ''PCR loop''. The PCR loop is designed to free the central bus during the time consuming PCR reaction. During PCR reaction, the droplets enter three temperature control zones and circulate along the PCR loop. The PCR loop is also connected to the detection zone in which the products can be detected at the end of each PCR cycle in a real-time PCR assay.

The architecture selected by Pan et al. would allow the user to be able to choose from different, specifically tailored SPU and RC units depending on the desired experiments. For example, the user may select the ''blood to DNA'' SPU for pathogen detection or the ''blood to RNA'' SPU for expression analysis. Similarly, the user could then purchase the specific RC kit such as the real-time PCR kit or flu detection kit. The SPU and RC manufacturers would follow certain standards for I/O interfacing and would provide drivers for the DMW to recognize a specific SPU

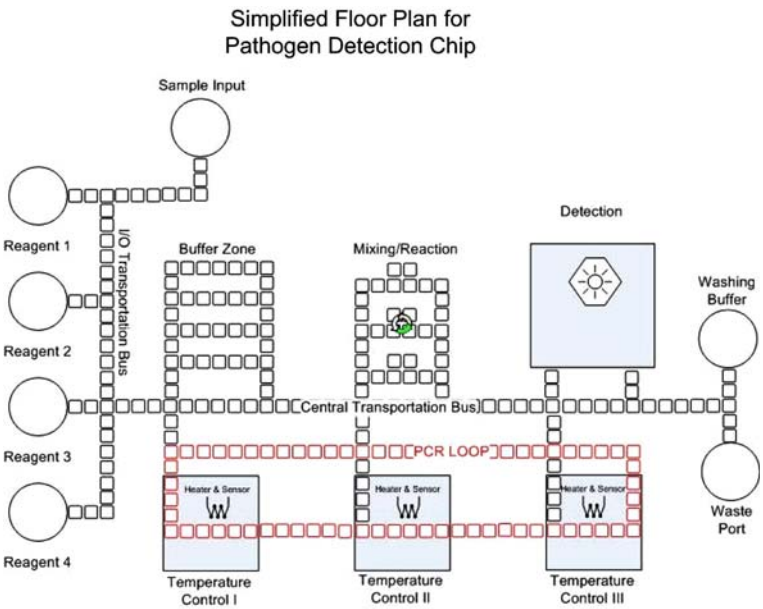

Fig. 46 DMW floor plan (Pan et al. 2006)

and RC. The biochip user would only need to connect SPU and RC to his DMW, load the suitable protocols, and the biochip would do the rest (Pan et al. 2006).

3.2 Detection of DNA using fiber optic spectroscopy

The second application is a EWD device capable of performing sample preparation, microanalysis, and the detection of specific, known DNA strands (Vijay et al. 2006). The entire system is intended to be compatible with a custom made cuvette that fits into a hand-held spectroscope. Thus, unlike the first application, all sample processing is performed in droplet form on an EWD platform. The input to the system is a sample of whole blood. Cell lyses is performed and specific DNA strands are separated. The DNA extract is then diluted and further amplified by PCR. The high-density DNA strands are separated through electrophoresis, and the output is mixed and the sample DNA binds with the potential complimentary DNA halves attached to gold nanoparticles. If the inputted DNA strand matches both halves of one of the potential compliments, the gold nanoparticle from each half will aggregate and create a visual change in the spectroscopic output of the system. A block diagram of the system is shown in Fig. 47.

The flowchart in Fig. 48 provides a comprehensive presentation of the overall functionality of the system.

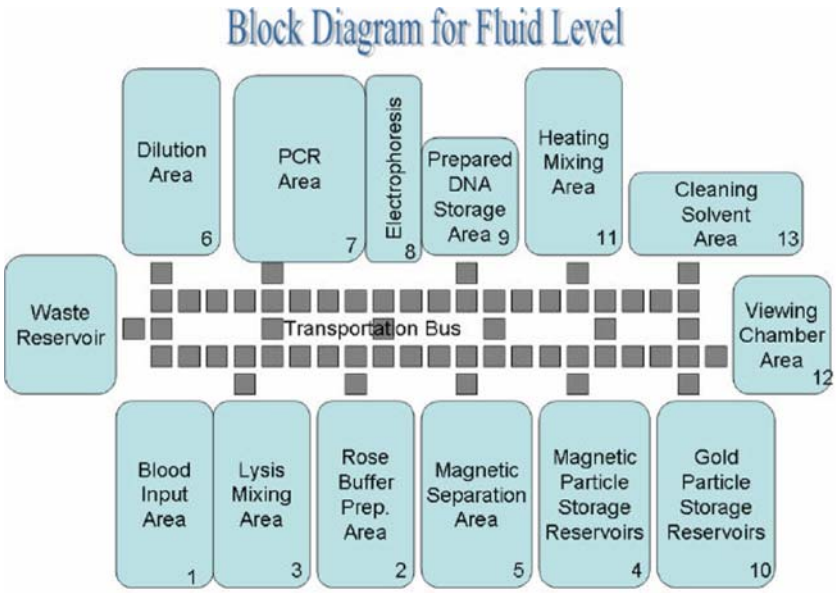

Fig. 47 Block diagram of the system. The areas shown here will be used in a specific order as described by the numbers in the boxes and the flow chart in Fig. 48 (Vijay et al. 2006)

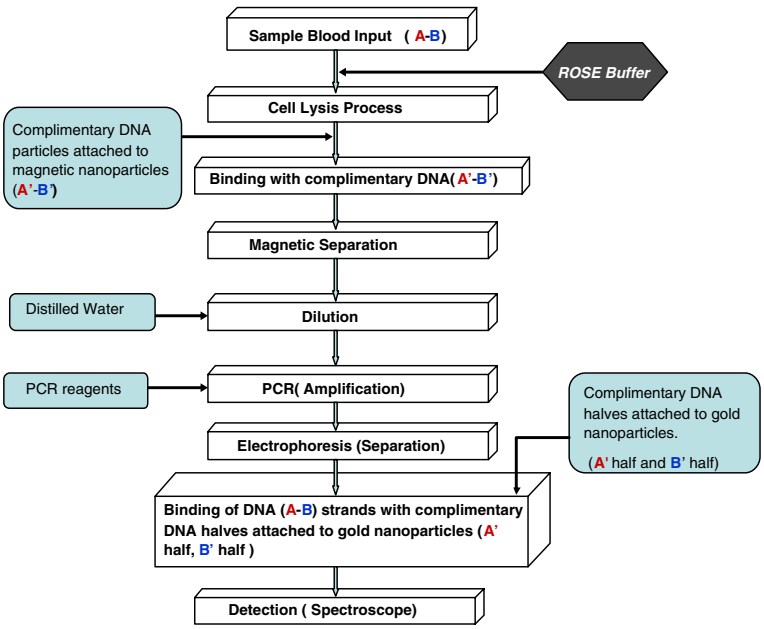

Fig. 48 This flowchart represents the general programming for the system. Overall, the sample will travel from input to detection by electrowetting (Vijay et al. 2006)

Each fluidic function in this chart is responsible for some general fluidic operation through the use of various EWD fluidic components. The blood sample is first drawn into the chip by using pressure-assisted droplet dispensing (Ren et al. 2003a, b) that creates 100 nl droplets (block 1, Fig. 47). The blood droplets are then moved to a blood reservoir that holds the sample before it undergoes cell lyses. From this reservoir 25 nl droplets will be pulled out, which requires smaller electrodes. Some of the key fluidic functions and operations are described below:

3.2.1 Cell lyses and DNA Attachment

Blood cell lysing is performed with a ROSE buffer solution. The buffer is mixed on-chip (Fig. 49a; block 2, Fig. 47) in droplet form by using the following reagents: 10 mM Tris–HCl, pH 8.0; 312.5 mM EDTA, pH 8.0; 1% sodium lauryl sarkosyl; and 1% polyvinylpolypyrrolidone (PVPP, water-insoluble). The blood droplet and the ROSE buffer are sent to the cell lysis mixing chamber (block 3, Fig. 47) where they mix by moving down the array in one direction to prevent reverse flow. This gives rise to the extracted DNA strand. The temperature of the chamber makes sure that the double DNA strand unwinds and forms single-stranded DNA. Once the single-stranded DNA (A–B) is extracted from the sample, the complimentary DNA strands (A′–B′) attached to magnetic nanoparticles are introduced and the temperature is lowered. The resulting DNA double strands obtained are sent to the magnetic separation chamber (block 5, Fig. 47). The remnants are sent to waste.

3.2.2 Magnetic separation, dilution, and PCR

The magnetic separation function is performed as follows: (1) the sample droplet is moved over a heater set to 95°C such that all DNA strands unbind; (2) the heater is turned off such that the DNA strands in the droplet can bind to the DNA strands on the magnetic beads; (3) the droplet is then moved under a permanent magnet attached to the top plate of the EWD device. All of the magnetic particles become clustered around the top of the droplet following the magnetic field gradients; (4) a series of wash droplets enter the area, exchange fluid with the droplet containing magnetic particles, and continue on to the waste reservoir. These droplets will slowly take away left-over cells and unimportant DNA strands; (5) once the excess particles have been sufficiently removed from the droplet, the heater will turn on again. When the heater turns on, the DNA strands in question will separate from the magnetic particles. The droplet containing the separated DNA will be transported to dilution and then to PCR for DNA amplification. The separation operation is illustrated in Fig. 50a. Dilution of the separated DNA (block 6, Fig. 47) occurs in a standard reservoir pre-filled with a specific volume of water to produce on the order of 1:169 dilution prior to PCR, as shown in Fig. 50b.

PCR (block 7, Fig. 47) is performed by passing the DNA sample and the reagents through three temperature zones where the DNA undergoes the processes of denaturing, annealing, and elongation. This completes one PCR cycle. To achieve high-degree of amplification, 20–35 of such cycles may be required. The DNA and the samples are transferred from one part of the PCR section to the other by electrowetting, as shown in Fig. 50c.

After PCR the droplet is transported to the electrophoresis area (block 8, Fig. 47), also described above in Fig. 35. The last two electrowetting pads in Fig. 35 are actually on the top plate. The droplet can still transport via the top electrodes. These electrodes bring the droplet above and in contact with the electrophoresis starting reservoir. Voltage is turned off on the pads such that the droplet settles onto the first electrophoresis reservoir. Then a voltage is applied across the electrophoresis capillary that starts pulling the liquid along the capillary due to the DNA's strong negative charge. As the DNA traverses, high density strands separate from low density strands. The DNA will need to be fluorescently tagged to detect plug

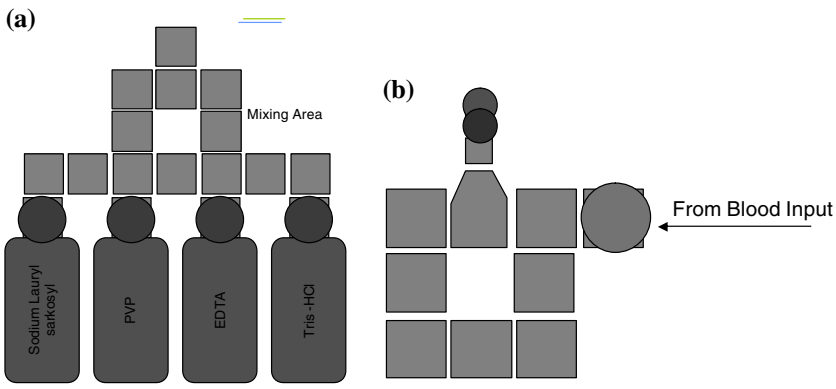

Fig. 49 **a** These four standard reservoirs contain the specific buffers to make the ROSE lyses solution. A total of 5 nl droplets will be combined, mixed, and split in order to form the correct make up of ROSE buffer, **b** This is the cell lysis area. It has both 25 and 5 nl sized electric pads. This necessitates a custom shaped electric pad that allows for proper combining of the two (Vijay et al. 2006)

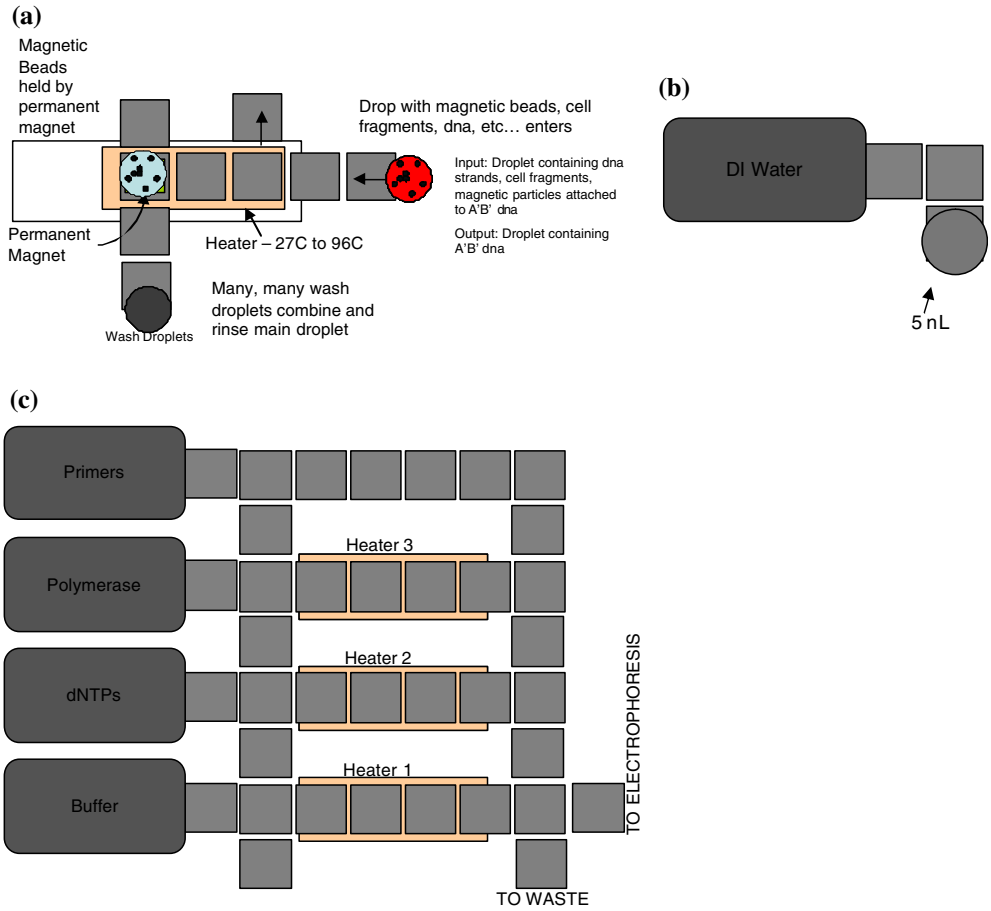

Fig. 50 **a** This is the magnetic separation area. Droplets enter from the right. There is a heater (*orange*) and a permanent magnet (*green*). Rinse droplets come from the bottom, waste goes out the top to the waste reservoir, and the end separated droplet is ultimately sent to the bus. **b** The dilution reservoir is a standard reservoir with a specific pre-filled amount of DI water. **c** This is a representation of the PCR area. There will be three heaters and five reservoirs. There will be sufficient electric pads to allow for proper transport (Vijay et al. 2006)

positions, allowing the electric field to be switched across the first of two perpendicular capillaries to catch the high density strands. This is done twice to reduce the volume from ~3 to 2 to 1 nl to make sure the right volume of ''plug'' is achieved. These strands will be completely separated from the low-density strands and will be pushed into the exit reservoir. The exit reservoir will have electrowetting electrodes on the top plate and will work exactly the same way as the input interface (Vijay et al. 2006).

3.2.3 DNA/gold binding and detection

A droplet from this exit reservoir (block 9, Fig. 47) is dispensed and mixed with a droplet from the first gold particle/compliment DNA strand reservoir (block 10, Fig. 47). Once properly mixed, the coalesced droplet containing gold particles and DNA will be moved to a heater (block 11, Fig. 47). This process breaks apart any double-stranded DNA segments. The heater is turned off, and as the heater cools the DNA strands bind to their compliments if they are present. This includes the DNA A–B to A′–B′ combination, which is the goal of this application. This process is repeated to improve the chances of binding of both halves of the complimentary to the DNA strand. The resulting fluid will be sent to the viewing chamber. If the DNA in question is present, the gold particles will be aggregated. Enough drops of the gold particle/DNA solution will be carted in to fill the viewing chamber reservoir. If the inputted DNA strand matches both halves of one of the potential compliments, the gold nanoparticle from each half will aggregate and create a visual change in the spectroscopic output of the system (Vijay et al. 2006). This process is diagrammed in Fig. 51.

3.3 Remarks on applications

The two ''paper designs'' described above support the notion that an extensive biomedical application base can be leveraged by expanding microfluidic operations based on electrowetting into a complete system. To create the microfluidic architectures described requires shared elemental fluidic operations (integration), reconfigurability, no cross-contamination, perhaps multitasking by components, and few bottlenecks. While these examples have not undergone the test of real implementation, nevertheless the fluidic operations described have been largely demonstrated in experiments. These designs show that a wide diversity in biomedical applications can be parsed into manageable

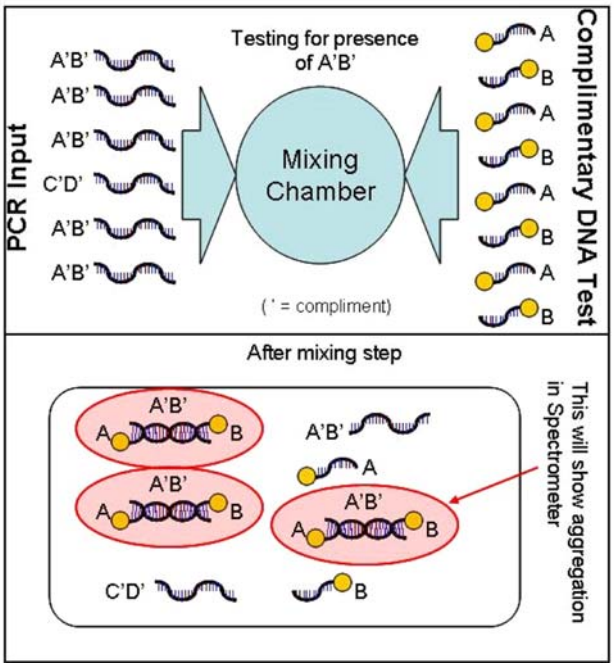

Fig. 51 *Top*: Before mixing takes place (block 11, Fig. 47), there is a droplet of DNA and one of gold-complimentary DNA. After the mixing (*bottom*), some of the gold-complimentary DNA binds to either side of the AB chain and cause aggregation (Vijay et al. 2006)

components and assembled into an architecture that is programmable, reconfigurable, and reusable. This capability opens the possibility of handling all of the protocols that a given laboratory or a class of applications would require. And, it provides a path toward realizing the true lab-on-a-chip.

4 Conclusions

At the present time there are over 25 groups worldwide working on droplet-based electrowetting science and technology, and the number of papers published each year in this specialty is growing exponentially. While progress is being made in furthering the understanding of electrowetting phenomena from a fundamental perspective (Mugele and Baret 2005), other efforts are underway exploring the applications, novel device structures, and computer-aided design methods that are possible in digital microfluidics. Efforts in all of these areas are necessary to put the field on a solid footing and to find the unique niche that the technology can fill.

Investigators have conducted extensive research on the basic principles and operations underlying the implementation of electrowetting-based digital microfluidic systems. The result is a substantial ''microfluidic toolkit'' of automated droplet operations, a sizable catalog of compatible reagents, and demonstrations of a few important biological assays. However, the lack of good on-chip sample preparation methods is currently the biggest impediment to commercial acceptability of microfluidic technologies, including digital microfluidics. Other issues include system integration and interfacing to other laboratory formats and devices, packaging, reagent storage, maintaining temperature control of the chip during field operation, and a scalable, compatible detector technology.

And finally, there has been no attempt to implement molecular separation onto a digital microfluidic platform. The number and variety of analyses being performed on chip has increased along with the need to perform multiple-sample manipulations. It is often desirable to isolate components that produce a signal of interest, so that they can be detected. Currently, mass separation methods, such as capillary electrophoresis, are not an established part of the digital microfluidic toolkit and integration of separation methods presents a significant challenge.

Acknowledgments The author acknowledges funding from the following sources that has enabled technology development and collaborative efforts across many disciplines: DARPA, NSF, NIH, Lord Foundation, Glaxo Smith Kline, and the Duke University Medical Center. In addition, substantial contributions are acknowledged by current and former students at Duke University whose contributions have helped establish significant progess in the application of EWD towards a useful end.

References

Abdel-Hamid I, Ivnitski D, Atanasov P, Wilkins E (1999) Flow-through immunofiltration assay system for rapid detection of *E. coli* O157:H7. Biosens Bioelectron 14:309–316

Aizenberg J, Krupenkin T, Kolodner P (2006) Accelerated chemical reactions for lab-on-a-chip applications using electrowetting-induced droplet self oscillations. Mater Res Soc Symp Proc 915:103–111

Anton DA, Valentino JP, Trojan SM, Wagner S (2003) Thermocapillary actuation of droplets on chemically patterned surfaces by programmable microheater arrays. J Microelectromech Syst 12:873–879

Bains W, Smith GC (1988) A novel method for nucleic acid sequence determination. J Theor Biol 135(3):303–307

Berge B (1993) Electrocapillarite et mouillage de films isolants par l'eau. C R Acad Sci II 317:157

Berthier J, Clementz Ph, Raccurt O, Jary D, Claustre P, Peponnet C, Fouillet Y (2006) Computer aided design of an EWOD microdevice. Sens Actuators A 127:283–294

Braslavsky I, Hebert B et al (2003) Sequence information can be obtained from single DNA molecules. Proc Natl Acad Sci USA 100(7):3960–3964

Brenner S, Williams SR et al (2000) In vitro cloning of complex mixtures of DNA on microbeads: physical separation of differentially expressed cDNAs. Proc Natl Acad Sci USA 97(4):1665–1670

Cady NC, Stelick S, Kunnavakkam MV, Liu Y, Batt CA (2004) A microchip-based DNA purification and real-time PCR biosensor for bacterial detection. Proc IEEE Sens 3:1191–1194

Chatterjee D, Boonta H, Wheeler AR, King J, Garrell RL (2006) Droplet-based microfluidics with nonaqueous solvents and solutions. Lab Chip 6:199–206

Cho S-K, Kim C-J (2003) Particle separation and concentration control for digital microfluidic systems. Proc IEEE Micro Electro Mech Syst (MEMS) 686–689

Cho S-K, Moon H, Fowler J, Kim C-J (2001) Splitting a liquid droplet for electrowetting-based microfluidics. In: Proceedings of 2001 ASME Inter Mech Eng Congress and Expo, November 11–16, New York, NY

Cho S-K, Fan S-K, Moon H, Kim C-J (2002) Towards digital microfluidic circuits: creating, transporting, cutting and merging liquid droplets by electrowetting-based actuation. Technical Digest MEMS 2002 IEEE International Conference on Micro Electro Mechanical Systems, vol 11, pp 454–461

Cho S-K, Moon H, Kim C-J (2003) Creating, transporting, cutting, and merging liquid droplets by electrowetting-based actuation for digital microfluidic circuits. J Microelectromech Syst 12(1):70–80

Chou H-P, Unger MA, Quake SR (2001) A microfabricated rotary pump. Biomed Microdevices 3(4):323–330

Cooney CG, Chen C-Y, Emerling MR, Nadim A, Sterling JD (2006) Electrowetting droplet microfluidics on a single planar surface. Microfluid Nanofluid 2:435–446

Deamer DW, Akeson M (2000) Nanopores and nucleic acids: prospects for ultrarapid sequencing. Trends Biotechnol 18:147–151

Deamer DW, Branton D (2002) Characterization of nucleic acids by nanopore analysis. Acc Chem Res 35:817–825

Delamarche E (1997) Patterned delivery of immunoglobulins to surfaces using microfluidic networks. Science 276:779–781

Delamarche E (1998) Microfluidic networks for chemical patterning of substrates: design and applications to bioassays. J Am Chem Soc 120:500–508

Ding J, Chakrabarty K, Fair RB (2001) Scheduling of microfluidic operations for reconfigurable two-dimensional electrowetting arrays. IEEE Trans Computer -Aided Des Integr Circuits Syst 29:1463–1468

Drmanac S (1998) Accurate sequencing by hybridization for DNA diagnostics and individual genomics. Nature Biotechnol 16:54–58

Emrich CA (2002) Microfabricated 384-lane capillary array electrophoresis bioanalyzer for ultrahigh-throughput genetic analysis. Anal Chem 74:5076–5083

Fair RB, Pollack MG, Woo R, Pamula VK, Ren H, Zhang T, Venkatraman J (2001) A microwatt metal-insulator-solution-transport (MIST) device for scalable digital bio-microfluidic systems. Technical Digest, International Electron Device Meeting, pp 367–370

Fair RB, Srinivasan V, Paik P, Ren H, Pamula VK, Pollack MG (2003) Electrowetting-based on-chip sample processing for integrated microfluidics. Technical Digest IEEE International Electron Dev Meeting, 2003, pp 779–782

Fair RB, Khlystov A, Srinivasan V, Pamula VK, Weaver KN (2004) Integrated chemical/biochemical sample collection, pre-concentration, and analysis on a digital microfluidic lab-on-a-chip platform. In: Smith LA, Sobek D (eds) Lab-on-a-chip: platforms, devices, and applications., Proceedings. Oof SPIE 5591, pp 113–124

Fair RB (2005) Dynamically reconfigurable surfaces for microfluidic applications. MRS Spring Meeting, San Francisco, CA

Fair RB, Khlystov A, Tailor T, Ivanov V, Evans RD, Srinivasan V, Pamula V, Pollack MG, Griffin PB, Zhou J (2007) Chemical and biological applications of digital-microfluidic devices. IEEE Des Test (in press)

Fan S-K, Hashi C, Kim C-J (2003) Manipulation of multiple droplets on nxm grid by cross-reference EWOD driving scheme and pressure-contact packaging. In: Proceedings of the IEEE 16thSixteenth annual interernational conference on micro electro mechanical sSystems, pp 694–697

Fang Q (2004) Sample introduction for microfluidic systems. Anal Bioanal Chem 378:49–51

Figeys D, Gygi SP, McKinnon G, Aebersold R (1998) An integrated microfluidics-tandem mass spectrometry system for automated protein analysis. Anal Chem 70:3728–3734

Fitzpatrick A (2006) Creating a rapid handheld malaria detection device for developing countries. Research project Duke University

Fodor SPA, Read JL et al (1995) Light-directed, spatially addressable parallel chemical synthesis. Science 251(4995):767–773

Fowler J, Moon H, Kim C-J (2002) Enhancement of mixing by droplet-based microfluidics. Proc IEEE MEMS 97–100

Gascoyne PRC, Vykoukal JV (2004) Dielectrophoresis-based sample handling in general-purpose programmable diagnostic instruments. Proc IEEE 92:22–42

Gong M, Kim CJ (2005) Two-dimensional digital microfluidic system by multilayer printed circuit board. In: 18th IEEE international conference on micro electro mechanical systems, pp 726–729

Griffith EJ, Srinivas A, Goldberg MK (2006) Performance characterization of a reconfigurable planar-array digital microfluidic system. IEEE Trans Comput Aided Des Integr Circuits and Syst 25:345–357

Harrison DJ, Fluri K, Chiem N, Tang T, Fan Z (1996) Micromachining chemical and biochemical analysis and reaction systems on glass substrates. Sens Actuators B Chem B33:105–109

He B, Burke BJ, Zhang X, Zhang R, Regnier FE (2001) A picoliter-volume mixer for microfluidic analytical systems. Anal Chem 73:1942–1947

Heim S, Schnieder I, Binz D, Vogel A, Bilitewski U (1999) Development of an automated microbial sensor system. Biosensors and Bioelectronics 14:187–193

Hessel V, Lowe H, Schoenfeld F (2005) Micromixers-a review on passive and active mixing principles. Chem Engrg Sci 60:2479–2501

Hinsmann P, Haberkorn M (2001) Time resolved FTIR spectroscopy of chemical reactions in solution in fast diffusion-based mixing in a micromachined flow cell. Appl Spectrosc 55:241–251

Hosokawa K, Fujii T, Endo I (1999a) Handling of picoliter liquid samples in a poly(dimethylsiloxane)-based microfluidic device. Anal Chem 71:4781–4785

Hosokawa K, Fujii T, Endo I (1999b) Droplet-based nano/picoliter mixer using hydrophobic microcapillary vent. Micro Electro Mech Syst 1999:388

Jacobson SC, McKnight TE, Ramsey JM (1999) Microfluidic devices for electrokinetically driven parallel and serial mixing. Anal Chem 71:4455–59

Jary D, Chollat-Namy A, Fouillet Y, Boutet J, Chabrol C, Castellan G, Gasparutto D, Pepponet C (2006) DNA repair enzyme analysis on EWOD fluidic microprocessor. NSTI Nanotech 2006 Technical Proceedings, vol 2, pp :554–557

Jones TB, Fowler JD, Chang YS, Kim C-J (2003) Frequency-based relationship of electrowetting and dielectrophoretic liquid microactuation. Langmuir 19:7646–7651

Jopling J (2001) Microfluidic architecture and biomedical applications simulation. MS Thesis, Duke University

Jurinke C, van den Boom D (2002) The use of MassARRAY technology for high throughput genotyping. Adv Biochem Eng Biotechnol 77:57–74

Kartalov EP, Quake SR (2004) Microfluidic device reads up to four consecutive base pairs in DNA sequencing-by-synthesis. Nucleic Acids Res 32:2873–2879

Koch M, Chatelain D (1998) Two simple micromixers based on silicon. J Micromech Microeng 8:123–126
Koutny L et al (2000) Eight hundred-base sequencing in a microfabricated electrophoretic device. Anal Chem 72:2288–3391
Lagally ET, Simpson PC, Mathies RA (2000) Monolithic integrated microfluidic DNA amplification and capillary electrophoresis analysis system. Sens Actuators B 63:138–146
Lee J, Moon H, Fowler J, Kim C-J, Schoellhammer T (2001) Addressable micro liquid handling by electric control of surface tension. In: Proceedings. of the 2001 IEEE 14th international conference on MEMS, Interlaken, Switzerland, pp 499–502
Li J, Gershow M (2003) DNA molecules and configurations in a solid-state nanopore microscope. Nat Mater 2:611–615
Lienemann J, Greiner A, Korvink JG (2006) Modeling, simulation, and optimization of electrowetting. IEEE Trans Comput Aided Des Integr Circuits Syst 25:234–247
Ligler FS, Anderson GP, Davidson PT, Foch RJ, Ives JT, King KD, Page G, Stenger DA, Whelen JP (1998) Remote sensing using an airborne biosensor. Environmental Sci Tech 32:2461–2466
Liu RH, Stremler MA, Sharp KV, Olsen MG, Santiago JG, Adrian RJ, Aref H, Beebe DJ (2000) Passive mixing in a three-dimensional serpentine microchannel. IEEE J Microelectromech Syst 9:190–197
Liu RH, Yang JN, Lenigk R, Bonanno J, Grodzinski P (2004) Self-contained, fully integrated biochip for sample preparation, polymerase chain reaction amplification, and DNA microarray detection. Anal Chem 76(7):1824–1831
Madou MJ, Cubicciotti R (2003) Scaling issues in chemical and biological sensors. Proc IEEE 91:830–838
Manz A, Graber N, Widmer HM (1990) Miniaturized total chemical analysis systems: a novel concept for chemical sensing. Sens Actuators B1:244–248
Margulies M, Egolm M et al. (2005) Genome sequencing in microfabricated high-density picolitre reactors. Nature 437(7057):376–380
Metzker ML, Raghavachari R et al (1994) Termination of DNA synthesis by novel 3′-modified-deoxyribonucleoside 5′-triphosphates. Nucleic Acids Res 22(20):4259–4267
Mitra RD, Butty VL et al (2003) Digital genotyping and haplotyping with polymerase colonies. Proc Natl Acad Sci USA 100(10):5926–5931
Moon H, Cho SK, Garrell RL, Kim CJ (2002) Low voltage electrowetting-on-dielectric. J Appl Phys 92:4080–4087
Moon H, Wheeler AR, Garrell RL, Loo JA, Kim C-J (2006) An integrated digital microfluidic chip for multiplexed proteomic sample preparation and analysis by MADDA-MS. Lab Chip 6:1213–1219
Mudsen BC, Murphy RJ (1981) Flow-injection and photometric-determination of sulfate in rainwater with methylthymol blue. Anal Chem 53:1924–1926
Mugele F, Baret JC (2005) Electrowetting: from basics to applications. J Phys Condens Matter 17:R705–R774
Mugele F, Baret J-C, Steinhauser D (2006) Microfluidic mixing through electrowetting-induced droplet oscillations. Appl Phys Lett 88:204106-1–3
Musyanovych A, Mailander V, Landfester K (2005) Miniemulsion droplets as single molecule nanoreactors for polymerase chain reaction. Biomacromolecules 6:1824–1828
Nagiel I (2006) Capacttive hysteresis curves in a microfluidic environment. ECE198 project Duke University
Nakane J, Broemeling D, Donaldson R, Marziali A, Willis TD, O'Keefe M, Davis RW (2001) A method for parallel, automayed, thermal cycling of submicroliter samples. Genome Res 11:441–447
Ottesen EA, Hong JW, Quake SR, Leadbetter JR (2006) Microfluidic digital PCR enables multigene analysis of individual environmental bacteria. Science 314(5804):1464–1467
Paegel BM, Blazej RG et al (2003) Microfluidic devices for DNA sequencing: sample preparation and electrophoretic analysis. Curr Opin Biotechnol 14:42–50
Paik PY (2006) Adaptive hot-spot cooling of integrated circuits using digital microfluidics. Ph.D. thesis, Duke University
Paik P, Pamula VK, Pollack MG, Fair RB (2003a) Electrowetting-based droplet mixers for microfluidic systems. Lab Chip 3:28–33
Paik P, Pamula VK, Fair RB (2003b) Rapid droplet mixers for digital microfluidic systems. Lab Chip 3:253–259
Paik PY, Pamula VK, Chakrabarty K (2004) Thermal effects on droplet transport in digitial microfluidics with applications to chip cooling. In: Thermomechanical phenomena in electronic systems—proceedings of the intersociety conference, v 1, ITherm 2004—9th intersociety conference on thermal and thermomechanical phenomena in electronic systems, pp 649–654
Pamula VK, Paik P, Venkatraman J, Pollack MG, Fair RB (2002) Microfluidic electrowetting-based droplet mixing. 2001 Microelectromech Syst Conf 8–10
Pamula VK, Pollack MG, Paik PY, Ren H, Fair RB (2005a) Apparatus for manipulating droplets by electrowetting-based techniques. US Patent 6,911,132, June 28, 2005
Pamula VK, Srinivasan V, Chakrapani H, Fair RB, Toon E (2005b) A droplet-based lab-on-a-chip for colorimetric detection of nitroaromatic explosives. In: 18th IEEE international conference on micro electro mechanical systems, pp 722–725
Pan G, Garcia A, Zhang J (2006) Analog/digital hybrid microfluidic chip for DNA & RNA Analysisanalysis. ECE299.01 class project, Duke University
Petersen KE, McMillan WA, Kovacs GTA, Northrup MA, Christel LA, Pourahmadi F (1998) Toward next generation clinical diagnostic instruments: scaling and new processing paradigms. Clinical Diag Inst 71–79
Pollack MG (2001) Electrowetting-based microactuation of droplets for digital microfluidics. Ph.D. thesis, Duke University
Pollack MG, Fair RB, Shenderov AD (2000) Electrowetting-based actuation of liquid droplets for microfluidic applications. Appl Phys Lett 77:1725–1727
Pollack MG, Shendorov A, Fair RB (2002) Electrowetting-–based actuation of droplets for integrated microfluidics. Lab Chip 2:96–101
Pollack MG, Paik PY, Shenderov AD, Pamula VK, Dietrich FS, Fair RB (2003) Investigation of electrowetting-based microfluidics for real-time PCR applications. In: 7thSeventh International conference on miniaturized chemical and biochemical analysis systems (μTAS 2003), Lake Tahao
Quilliet C, Berge B (2002) Investigation of effective interface potentials by electrowetting. Europhys Lett 60:99–105
Ramsey JM, van Den Berg A (eds). (2001) Micro total analysis systems. Kluwer, Monterey
Ren H (2004) Electrowetting-based sample preparation: an initial study for droplet transportation, creation and on-chip digital dilution. Ph.D. Tthesis, Duke University
Ren H, Srinivasan V, Fair RB (2003a) Design and testing of an interpolating mixing architecture for electrowetting-based droplet on-chip chemical dilution. In: 12th International conference-Inter Conf on solid-state sensors, actuators and microsystems. Digest of Technical Papers, pp 619–622
Ren H, Srinivasan V, Fair RB (2003b) Automated electrowetting-based droplet dispensing with good reproducibility. Proceedings of MicroTAS 2003:993–996

Renaudin A, Tabourier P, Zhang V, Druhon C, Camart JC (2004) ''Plateforme SAW dédiée à la microfluidique discrète pour applications biologiques''., In: 2ème Congrès Français de Microfluidique, Société Hydrotechnique de France, Toulouse, France, pp 14–16

Rohr T, Yu C, Davey M, Svec F, Frechet J (2001) Porous polymer monoliths: simple and efficient mixers prepared by direct polymerization in the channels of microfluidic chips. Electrophoresis 22:3959–3967

Ronaghi M (2001) Pyrosequencing sheds light on DNA Sequencing. Genome Res 11:3–11

Ruzicka J (1998) Bioligand interaction assay by flow injection absorptiometry using a nenewable biosensor system enhanced by spectral resolution. The Analyst 123:1617–1623

Schmalzing D (1997) DNA typing in thirty seconds with a microfabricated device. Proc Nat Acad Sci USA 94:10273–10278

Schneegass I, Brautigam R, Kohler JM (2001) Miniaturized flow-through PCR with different template types in a silicon chip thermocycler. Lab Chip 1:42–49

Schwartz LW, Roy RV, Eley RR, Princen HM (2004) Surfactant-driven motion and splitting of droplets on a substrate. J Eng Math 50:157–175

Seinfeld JH, Pandis SN (1998) Atmospheric chemistry and physics: from air pollution to climate change. Wiley, New York

Seyrat E, Hayes RA (2001) Amorphous fluoropolymers as insulators for reversible low-voltage electrowetting. J Appl Phys 90:1383–1386

Shoffner MA, Cheng J, Hvichia G, Kricka L, Wilding P (1996) Chip PCR. I. Surface passivation of microfabricated silicon-glass chips for PCR. Nucleic Acids Res 24:375–379

Squires TM, Quake SR (2005) Microfluidics: fluid physics at the nanoliter scale. Rev Mod Phys 77:977–1026

Srinivasan V (2005) A digital microfluidic lab-on-a-chip for clinical applications. Ph.D. thesis, Duke University

Srinivasan V, Pamula VK, Pollack MG, Fair RB (2003a) Clinical diagnostics on human whole blood, plasma, serum, urine, saliva, sweat, and tears on a digital microfluidic platform. Proc MicroTAS 2003:1287–1290

Srinivasan V, Pamula VK, Rao KD, Pollack MG, Izatt JA, Fair RB (2003b) 3-D Imaging of moving droplets for microfluidics using optical coherence tomography. In: 7thSeventh International conference on miniaturized chem and biochem anal systems (μTAS 2003), Lake Tahao

Srinivasan V, Pamula VK, Paik PY, Fair RB (2004a) Protein stamping for MALDI mass spectrometry using an electrowetting-based microfluidic platform, In: Smith LA, Sobek D (eds) in lLab-on-a-chip: platforms, devices, and applications. Proc. of SPIE 5591, pp 26–34

Srinivasan V, Pamula VK, Fair RB (2004b) A droplet-based microfluidic lab-on-a-chip for glucose detection. Anal Chim Acta 507:145–150

Staicu A, Mugele F (2006) Electrowetting-induced oil film entrapment and instability. Phys Rev Lett 97:16780–16784

Stryer L (1995) Biochemistry, 4th edn. W.H. Freeman, New York

Su F, Chakrabarty K, Fair RB (2006) Microfluidics-based biochips: technology issues, implementation platforms, and design automation challenges. IEEE Trans Computer- Aided Des Of Integr Circuits. And Syst 25:211–223

Terrier F (1982) Rate and equilibrium studies in Jackson–Meisenheimer complexes. Chem Rev 82:77–152

Tian H, Huhmer AFR, Landers JP (2000) Evaluation of silica resins for direct and efficient extraction of DNA from complex biological matrices in a miniaturized format. Anal Biochem 283:175–191

Tokoro M, Katayama T, Taniguchi T, Torii T, Higuchi T (2002) PCR using electrostatic micromanipulation. In: Proceedings of the 41st SICE annual conference, vol 2, pp :954–956

Trinder P (1969) Determination of blood glucose using 4- amino phenazon as oxygen acceptor. J Clinical Pathology 22:246

Tulock JJ, Shannon MA, Bohn PW, Sweedler JV (2004) Microfluidic separation and gateable fraction collection for mass-limited samples. Anal Chem 76:6419–6425

V-Dinh T (1998) Development of a DNA biochip: principle and application. Sens Actuators B 51:52–59

Verheijen HJJ, Prins MWJ (1999) Reversible electrowetting and trapping of charge: model and experiments. Langmuir 15:6616–6620

Vijay A, Mathew N, Erb R (2006) Detection of the presence of a specific DNA strand using fiber optic spectroscopy. ECE299.01 class project, Duke University

Wainright A, Nguyen UT, Bjornson T, Boone TD (2003) Preconcentration and separation of double stranded DNA fragments by electrophoresis in plastic microfluidic devices. Electrophoresis 24:3784–3792

Walker SW, Shapiro B (2006) Modeling the fluid dynamics of electrowetting on dielectric (EWOD). J Microelectromechanical Syst 15:986–1000

Walker PA, Morris MD, Burns MA, Johnson BN (1998) Isotachophoretic separations on a microchip: normal Raman spectroscopy detection. Anal Chem 70(18):3766–3769

Wang W, Li Z-X, Luo R, Lu S-H, Xu A-D, Yang Y-J (2005) Droplet-based micro oscillating-flow PCR chip. J Micromech Microeng 15:1369–1377

Wheeler AR, Moon H, Kim C-J, Loo JA, Garrell RL (2004) Electrowetting-based microfluidics for analysis of peptides and proteins by matrix-assisted laser desorption/ionization mass spectrometry. Anal Chem 76:4833–4838

Wheeler AR, Moon H, Bird CA, Orgazalek Loo RR, Kim C-J, Loo JA, Garrell RL (2005) Digital microfluidics with in-line sample purification for proteomics analyses with MALDI-MS. Anal Chem 77:534–540

Wolfe KA, Breadmore MC, Ferrance JP, Power ME, Conroy JF, Norris PM, Landers JP (2002) Toward a microchip-based solid-phase extraction method for isolation of nucleic acids. Electrophoresis 23:727–733

Yi U-C, Kim C-J (2003) Soft printing of droplets digitized by electrowetting. Transducers 2003:1804–1808

Yi U-C, Kim C-J (2006) Characterization of electrowetting actuation on addressable single-side coplanar electrodes. J Micromech Microeng 16:2053–2059

Yoon J-Y, Garrell RL (2003) Preventing biomolecular adsorption in electrowetting-based biofluidic chips. Anal Chem 75:5097–5102

Zeng J (2006) Modeling and simulation of electrified droplets and its application to computer-aided design of digital microfluidics. IEEE Trans Comput Aided Des Integr Circuits Syst 25:224–233

Zeng J, Korsmeyer F (2004) Principes of droplet electrohydrodynamics for lab-on-a-chip. Lab Chip 4:265–277

Zhang T, Chakrabarty K, Fair RB (2002) Microfluidic systems modeling and simulation. CRC Press, Boca Raton

Zhang T, Chakrabarty K, Fair RB (2004) Behavioral modeling and performance evaluation of microelectrofluidics-based PCR systems using System C. IEEE Trans Comput -Aided Des Integr Circuits and Syst 23:843–858

Zhao Y, Cho SK (2006) Microparticle sampling by electrowetting-actuated droplet sweeping. Lab Chip 6(1):137–144